J. Fluid Mech. (1982), *vol.* 119, *pp.* 173–217
Printed in Great Britain

On the mechanism of wall turbulence

By A. E. PERRY AND M. S. CHONG
Department of Mechanical Engineering, University of Melbourne, Parkville, Victoria 3052, Australia

(Received 20 March 1981 and in revised form 17 July 1981)

In this paper an attempt is made to formulate a model for the mechanism of wall turbulence that links recent flow-visualization observations with the various quantitative measurements and scaling laws established from anemometry studies. Various mechanisms are proposed, all of which use the concept of the horse-shoe, hairpin or 'Λ' vortex. It is shown that these models give a connection between the mean-velocity distribution, the broad-band turbulence-intensity distributions and the turbulence spectra. Temperature distributions above a heated surface are also considered. Although this aspect of the work is not yet complete, the analysis for this shows promise.

1. Introduction

Recently, Head & Bandyopadhyay (1981) have shown by very convincing flow-visualization studies with smoke that a turbulent boundary layer consists of a 'forest' of hairpin vortices. These vortices can be seen in the ciné film of Bandyopadhyay & Head (1979) to lean in the downstream direction at approximately 45°, and all points on a given vortex appear to be convected with a uniform streamwise velocity. These vortices are undergoing a stretching motion, but remain approximately straight, implying a uniform stretching. They do not appear to be interacting strongly with each other. As the Reynolds number of the flow is increased, these vortices become finer and more densely packed. Head & Bandyopadhyay suggest that the lateral dimensions of the vortices follow the Kline scaling (see Kline 1967; Kline *et al.* 1967).

The present authors have also observed these vortices. Perry, Lim & Teh (1981) have observed similar vortices in turbulent spots and behind trip wires. Head & Bandyopadhyay make a distinction between vortex loops, horseshoe and hairpin vortices, all of which are topologically equivalent but are at different stages of stretching. We will simply refer to these vortices as 'Λ' vortices.

There is considerable evidence that these vortices originate from the wall in fully turbulent flow; see e.g. Corrsin (1957), Blackwelder (1978), and also Bakewell & Lumley (1967) who refer to 'counter-rotating vortex pairs of elongated streamwise extent' in the wall region of the flow. To quote Head & Bandyopadhyay: 'Further work in this area is evidently still required, but the present results certainly provide some experimental support for the ideas of Willmarth (1975, 1978) and Blackwelder (1978) and make it seem very likely that the hairpins or vortex pairs that are a prominent feature of the boundary layer as a whole have their origin in longitudinal vortex motions very close to the wall'. Head & Bandyopadhyay believe that they have seen these Λ-vortices form at the wall. Recently, a colleague, Dr T. T. Lim,

Law	Conditions	Some of the sources	Credibility
(1) $\frac{d\bar{U}_1}{dz} = \frac{U_\tau}{\kappa z}$	$z_+ \geqslant 100$, $z/\Delta_E \leqslant 0{\cdot}1$	Millikan (1938) by dimensional analysis based on a large amount of data; also Coles & Hirst (1968)	High
(2) $\frac{d\bar{\theta}}{dz} = \frac{\theta_\tau}{\kappa_H z}$	$z_+ \geqslant 100$, $z/\Delta_E \leqslant 0{\cdot}1$, $\sigma = O(1)$	Perry, Bell & Joubert (1966); Kadar & Yaglom (1972); Hoffmann & Perry (1979); Reynolds, Kays & Kline (1958)	Fairly high
(3) $\frac{d\overline{u_1^2}}{dz} = -\frac{A_{u_1} U_\tau^2}{z}$	$z_+ \geqslant 100$, $z/\Delta_E \leqslant 0{\cdot}1$	Townsend's (1976) attached-eddy hypothesis; Perry & Abell's (1977) spectral-similarity arguments and measurements	Fair since reliable measurements exist
(4) $\frac{d\overline{u_2^2}}{dz} = -\frac{A_{u_2} U_\tau^2}{z}$	$z_+ \geqslant 100$, $z/\Delta_E \leqslant 0{\cdot}1$	Townsend's (1976) attached-eddy hypothesis	Uncertain; no reliable measurements, but based on same hypothesis as 3
(5) $\frac{d\overline{u_3^2}}{dz} = 0$	$z_+ \geqslant 100$, $z/\Delta_E \leqslant 0{\cdot}1$	Townsend's (1976) attached-eddy hypothesis	Uncertain; no reliable measurements, but based on same hypothesis as 3
(6) Laws 1 and 3 work on a rough wall		Perry & Abell (1977); Hama (1954); Clauser (1956)	Law 1 high; law 3 fair; needs more work

TABLE 1. A selection of 'facts' about wall turbulence. Here $\bar{U}_1$ is the mean velocity, z is the distance normal to the wall, U_τ is the friction velocity, $\bar{\theta}$ is the mean temperature, θ_τ is the friction temperature, u_1, u_2 and u_3 are fluctuating velocities, and $\kappa \simeq \kappa_H$, A_{u_1} and A_{u_2} are universal constants, $z_+ = zU_\tau/\nu$, where ν is the kinematic viscosity. Δ_E is the boundary-layer thickness and σ is the Prandtl number. The overbar denotes time average.

believes he has also seen this formation in a fully turbulent flow, and this work is still continuing. This formation is difficult to observe (see § 5.3).

Once these vortices are formed they appear to undergo a stretching motion until they become highly elongated vortex pairs. This process was seen very clearly by Perry, Lim & Teh in the vortices behind trip wires.

Thus a turbulent boundary layer appears to have a granular structure with a characteristic direction. The large-scale 'bulge' observed with intermittency detectors could well be a 'colony' of fine-scale Λ-vortices passing the sensing probe.

The idea of modelling the turbulent boundary layer with a random array of Λ-vortices is not new and has been discussed since Theodorsen (1952, 1954) published his papers. However, the evidence for the existence of these vortices is now much stronger, and it appears that the time is ripe to consider this proposal seriously. The Λ-vortex is a perfect candidate for the Townsend's (1976) attached-eddy hypothesis. Townsend does not commit himself as to the nature of his geometrically similar eddies, but proposed that the eddies that contribute strongly to the Reynolds shear stress at a given height z above the boundary, scale with that height and are therefore 'in a sense, attached to the wall'. We believe that with the Λ-vortices one has all the necessary ingredients for linking the mean-velocity field with the Reynolds shear stress, broad-band turbulence, spectra and even the entrainment processes. Such

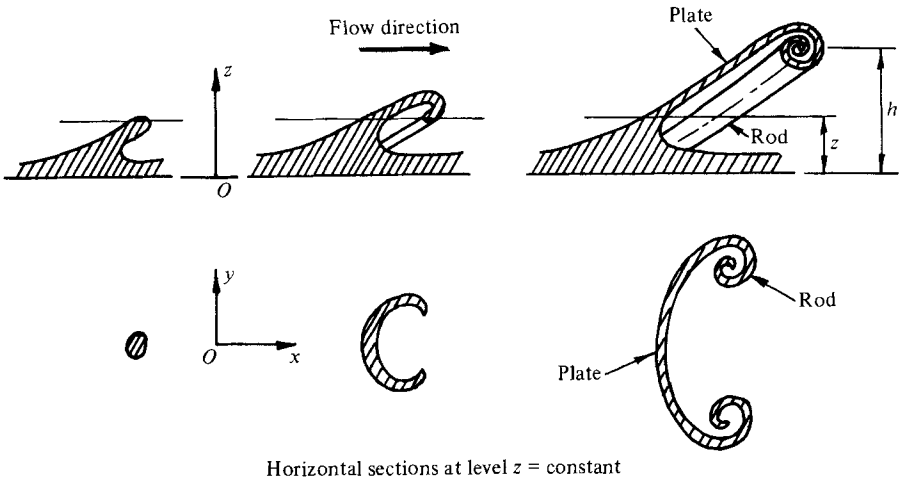

FIGURE 1. Birth of a young eddy.

modelling also shows promise in obtaining the link between mean-temperature fields and velocity fields in the presence of heat transfer from the wall. There are many directions or 'scenarios' that need to be pursued regarding the motion and scaling of these vortices. Existing laws for mean flow, broad-band turbulence and spectra established from hot-wire anemometry and Pitot-tube investigations are used here as a guide for narrowing down these possible directions. Unfortunately, in spite of the enormous literature on anemometry and Pitot-tube measurements of wall turbulence, very few reliable 'facts' emerge. The authors have selected a few facts that have reasonably convincing experimental support. These are listed in table 1, together with a 'credibility rating'. Some symbols are also defined in the table.

Figure 1 shows the conjectured birth of an eddy from the viscous-sublayer material. This material forms a sheet which rolls up at the edges. A series of horizontal cross-sections are shown in figure 1. For convenience, we have divided the vortex sheet into 'plates' and 'rods' of vorticity. The flow pattern about such a vortex is discussed later in more detail, but, from the work of Perry, Lim & Chong (1980) and from considerations in § 3, the conjectured pattern seen by an observer moving with the vortex is shown in figure 2. The 'saddle–node combination' sets up a flow which lifts vortex filaments from the surface and wraps them into rods. Such a 'combination' has been deduced to exist by the above authors in coflowing wake patterns using the theorems of critical-point theory. It is conjectured that most of the cross-stream component of vorticity resides in the rods once the roll-up of the vortex is complete. It will be shown in § 3 that the vortex undergoes a stretching motion by the Biot–Savart law, and this stretching helps to dissipate energy. In figure 2, the rods of vorticity are rounded at their apex, as has been observed by Head & Bandyopadhyay. In much of the analysis which follows, horizontal sectionings of the rods are used for calculating the mean-vorticity distributions. A rounded-top eddy causes considerable mathematical complexity in describing the sectioning at the apex; therefore for simplicity the rods will be assumed to merge at a sharp point. Although this is an approximation it makes the mathematics tractable. It turns out that, in some of the models, the precise shape of the Λ-vortex is not important.

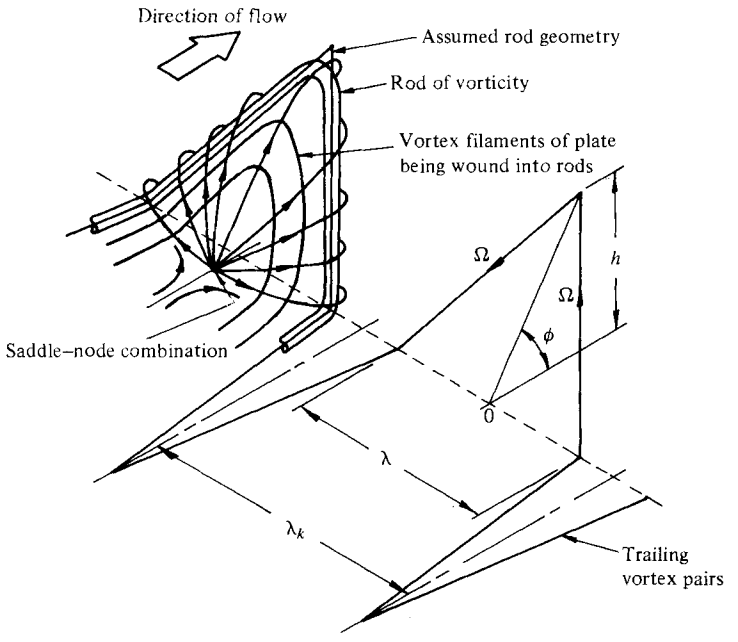

FIGURE 2. Λ-vortex configuration.

The diagram shown in figure 2 was inspired by the observations of trip-wire and turbulent-spot vortices. The tails of turbulent spots were interpreted by Perry, Lim & Teh as being trailing vortex pairs running along the wall and originating from initially spanwise-orientated vorticity. These could be related to the motions discussed by Bakewell & Lumley (1967).

It will be shown that the stretching motion brings the legs of the Λ-vortex together, i.e., as h increases, λ decreases. It is then quite plausible that viscous diffusion will lead to vorticity cancellation, leading to the 'death' of an eddy. Thus one major simplification is that the Λ-vortices are surrounded by irrotational fluid. Although this might not be precisely true, it is necessary before any tractable analysis can proceed.

It will be seen later that these vortex rods undergo a local axisymmetrical straining motion; the diffusion of vorticity and heat under this condition will need to be examined – this is done in § 2. In § 3 the details of the flow patterns surrounding the eddy and its straining motions are analysed using the Biot–Savart law. In § 4 a simple model for the mean flow and temperature distribution is proposed for a turbulent boundary layer, assuming that all the eddies scale according to the Kline scaling. However, it will be shown in § 5 that such a simple model is not possible, because the height of the eddy is limited by its 'death', and that it is necessary for a hierarchy of scales of eddies to exist in order to extend the region of validity of the logarithmic law of the wall to arbitrary high z_+ values for increasing Reynolds numbers. In § 6 the broad-band turbulent-intensity distributions are derived. The analysis is similar to that of Townsend, except that non-geometrically similar eddies, caused by the stretching motions, are included. In § 7 the spectral laws are derived using the Biot–Savart law for generating the 'signatures' of the eddies.

With the use of the Λ-vortex concept, a unified theory of wall turbulence can be constructed that links the mean flow with the Reynolds shear stress, turbulent-intensity distributions and spectra.

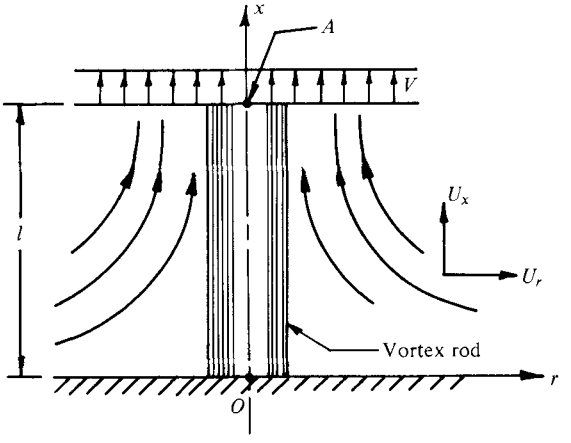

FIGURE 3. Vortex rod undergoing axisymmetrical strain.

2. The diffusion of vorticity and heat from stretched vortex rods

One important aspect of turbulence is the stretching of the vortex rods. How does vorticity and heat diffuse as the rod is being stretched and at what rate of stretching can this diffusion be suppressed? The stretching of rods is one mechanism by which viscous dissipation takes place.

Consider for simplicity a straight rod of vorticity being stretched by axisymmetrical strain. This could be simulated by placing the rod of vorticity at an axisymmetrical stagnation point as shown in figure 3. This will introduce swirl, and the rod will undergo a stretching motion. The vorticity transport equation is

$$\frac{\partial \boldsymbol{\Omega}}{\partial t} + (\mathbf{U}.\nabla)\,\boldsymbol{\Omega} = (\boldsymbol{\Omega}.\nabla)\,\mathbf{U} + \nu\nabla^2\boldsymbol{\Omega}, \tag{2.1}$$

where $\boldsymbol{\Omega}$ is the vorticity vector and $\mathbf{U}$ is the velocity vector located by co-ordinates r and x in figure 3. Axisymmetric strain is given by

$$U_x = 2kx, \quad U_r = -kr, \tag{2.2}$$

where U_x and U_r are the axial and radial components of velocity respectively, and k is a constant. From (2.1) a 'smeared-out' vorticity similarity solution can be found of the form

$$\Omega/\Omega_1 = f(\gamma), \tag{2.3}$$

where

$$f(\gamma) = 1 - \tfrac{1}{2}\gamma^2 + \tfrac{1}{2}\tfrac{1}{4}\gamma^4 - \tfrac{1}{2}\tfrac{1}{4}\tfrac{1}{6}\gamma^6 + \ldots$$

$$= \exp(-\tfrac{1}{2}\gamma^2), \tag{2.4}$$†

where Ω is the modulus of the vorticity at radius r, and Ω_1 is the corresponding value at $r = 0$. Ω_1 is a function of time. All vorticity is directed in the x-direction. The quantity $\gamma = r/r_0$, where r_0 is a length scale of the vorticity distribution; γ is a function of time. In fact, r_0 is given by

$$r_0 = \left(\frac{\nu}{k}\right)^{\frac{1}{2}} \left\{1 - e^{-2kt} + \frac{k r_0^2(0)\, e^{-2kt}}{\nu}\right\}^{\frac{1}{2}}, \tag{2.5}$$

where $r_0(0)$ is the initial length scale of the rod (radius) and t is time.

† Townsend (1951*a*, *b*) arrived at this equation from a similar analysis.

So far we have considered a constant value for k. This corresponds to exponential stretching since a length l of a marked portion of the rod (shown in figure 3) increases exponentially with time. Also the velocity of a marked particle A increases exponentially with time. If the rod is stretched at a uniform velocity V, i.e. if l increases uniformly with time, then k becomes time dependent and is given by

$$k = \frac{V}{2(x_0 + Vt)}, \tag{2.6}$$

where x_0 is the initial length of the rod. The solution (2.4) is unaffected by this different strain variation, but r_0 is now given by

$$r_0 = \left[\frac{2\nu(x_0 t + \frac{1}{2}Vt^2) + x_0 r_0^2(0)}{x_0 + Vt}\right]^{\frac{1}{2}}. \tag{2.7}$$

For the case of exponential stretching a characteristic time scale $\hat{t}$ is given by

$$\hat{t} = \frac{1}{2k} \ln\left\{\frac{kr_0^2(0)}{\nu} + 1\right\}. \tag{2.8}$$

When $t \ll \hat{t}$, the behaviour of the rod is inviscid. From (2.5), the rod radius decreases exponentially with time. Also it can be shown that the vorticity increases exponentially with time. However, no matter how small the viscosity, there will be a time ($t = O(\hat{t})$, see (2.5)) when viscosity has an influence. In fact, if $t \gg \hat{t}$, Ω_1 remains constant and so also does the rod radius r_0. In this situation, viscous-diffusion effects and the stretching effects are in balance.

In the case of uniform stretching, a new time scale τ can be derived from (2.7):

$$\tau = \frac{r_0(0)}{V}[\Phi + (\Phi^2 + R)^{\frac{1}{2}}], \tag{2.9}$$

where $\Phi = x_0/r_0(0)$ and $R = Vx_0/\nu$. Uniform stretching is the situation most likely to occur in wall turbulence, and a balance between diffusion and stretching is never achieved. Viscous diffusion will ultimately dominate and r_0 will ultimately follow the law

$$r_0 = (\nu t)^{\frac{1}{2}}. \tag{2.10}$$

For $t \ll \tau$, again the vortex rod will behave inviscidly.

A similar analysis can be applied for temperature distributions. If we imagine the rod to be elevated in temperature above the surrounding fluid, the analysis shows that the behaviour for temperature is much the same as for vorticity.

The above results are useful in understanding the 'death' processes of an eddy and could be incorporated in the spectral analysis given later.

3. Application of the Biot–Savart law to a Λ-vortex

It is instructive to examine how an isolated Λ-shaped vortex deforms under its own self-induced velocity with its image in the wall. The surrounding vector field generated by this vortex is of interest since it gives an insight into the entrainment and transport processes. It will be assumed that the flow is inviscid and that slip is allowed at the boundary. Physically, this slip is generated by the presence of the thin viscous sublayer. The only effect of the sublayer is to allow an arbitrary translation of the flow relative

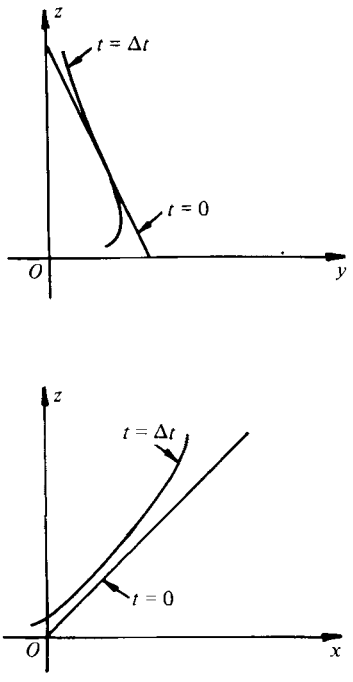

FIGURE 4. Deformation of Λ-vortex after one time step; only one leg is shown.

to the rigid boundary. These boundary conditions are used by Townsend in his attached-eddy hypothesis (1976). As mentioned earlier, the surrounding fluid is irrotational, since all vorticity in the mean flow is assumed to be contained in the rods. The rods are of finite diameter but, for computing the flow field outside the rods using the Biot–Savart law, the rod diameter can be regarded as zero. The trailing vortices at the boundary and their images are ignored, since these form dipoles of vorticity (i.e. vortex pairs) and their far-field effect is negligible. It will be seen that vortex interaction is small. Hence the far field for our isolated vortex will be assumed to be uniformly at rest for the purposes of applying the Biot–Savart law. The actual translational velocity in the far field relative to the boundary is irrelevant.

For simplicity the vortex filaments or rods will be assumed to be straight, since this enables analytical integrals to be obtained using the Biot–Savart law. Figure 2 shows the assumed geometry. The induced velocity at points located along the axis of any given rod can be readily computed by eliminating the rod in question and computing the effect of the other three rods (two of which are images). Knowing the velocities, the displacement of the rod after a short time interval Δt can be computed. A typical result is shown in figure 4. Except for the ends, where there are singularities, the rods appear to remain straight. It should be noted that the Λ-vortex is convecting itself backwards relative to the stream at infinity.

To avoid computational difficulties with curved rods, the updated position of the rods were assumed to be straight. This was done by drawing a straight line between two points on the middle third of the rod length, and extrapolating to the boundary and to the apex. This was then used for computing the next position of the rods in the next time step. Although this is crude, it was felt to be justified since the effects of

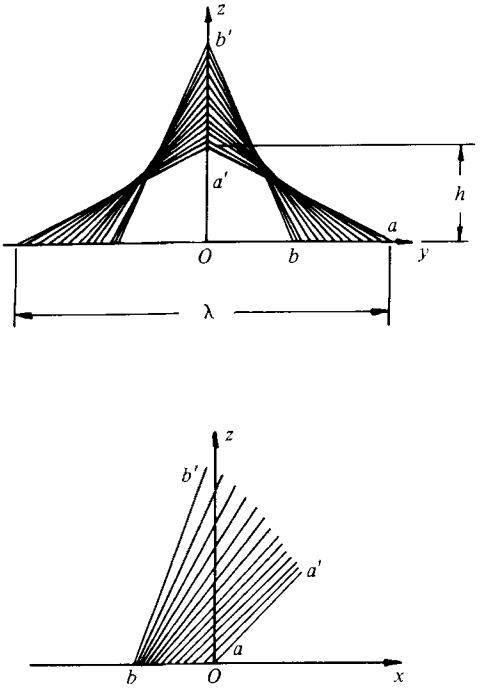

FIGURE 5. Deformation of Λ-vortex after a number of time steps. Initial value of $h/\lambda = \frac{1}{2}$ and $\phi = 45°$. a–a', initial position; b–b', final position.

the singularities at the ends of the rods (which in reality are not present) decay very rapidly with distance and have little effect over the central length. One could replace the sharp apex with a number of short straight sections of rods. This would introduce a series of weaker singularities. However, we contend that this would make little difference to the overall flow field outside the rods. Figure 5 shows the (y, z)-projection, and it can be seen that the Λ-vortex deforms in an approximate 'plane-strain' manner in the (y, z)-plane, i.e. the product λh remains roughly constant. Furthermore, the velocity of growth of h remains approximately constant. However, the angle of the (x, z)-projection increases. Whether the observed constant ϕ is caused by a restraining influence of neighbouring Λ-vortices is not known at this stage.

Figure 6(a) shows the instantaneous velocity vector field on the plane of symmetry of the Λ-vortex in the (x, z)-plane as seen by an observer at rest relative to the fluid at infinity. One can see that the induced velocity drops off very rapidly. The rods form a vortex pair in the (x, y)-plane (see later) and the vector field, in the large, resembles a dipole. Thus we would expect very little interaction with neighbouring Λ-vortices.† In figure 6(b) we have shown only the directions of the vectors.

Figure 6(c) shows the same vector field relative to an observer moving with the convection velocity of the Λ-vortex as computed at the mid-point within the rods, i.e. $z/h = \frac{1}{2}$. The geometry of the flow field is shown more clearly in figure 6(d), where only the directions are shown.

Figure 7a, b shows the patterns of the (x, y)-plane (the wall) as seen by an observer

† Of course this difficult problem of vortex interaction should be studied in further refinements of this modelling.

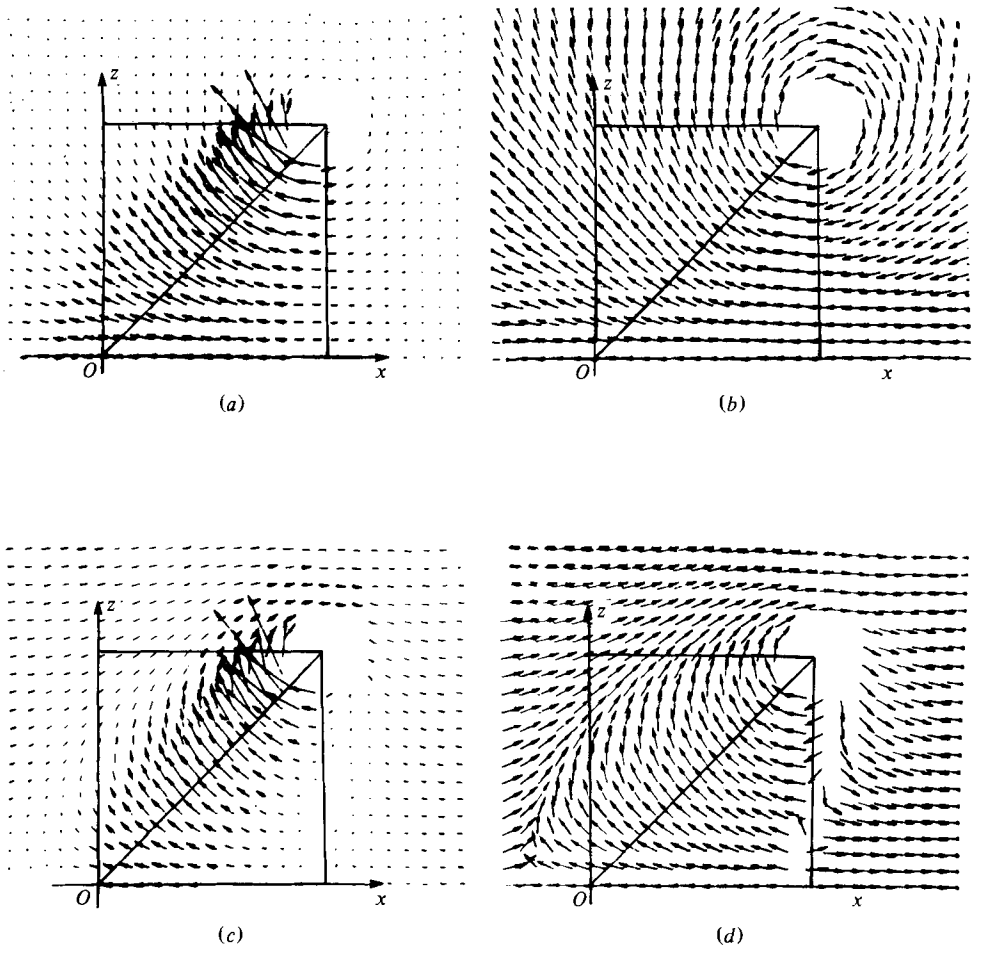

FIGURE 6. Velocity field at plane of symmetry ((x, z)-plane) of Λ-vortex. (*a*) Velocity field relative to observer at rest relative to fluid at infinity. (*b*) As (*a*) but with only velocity directions indicated. (*c*) Velocity field relative to observer moving with convection velocity of Λ-vortex. (*d*) As (*c*) but with only velocity directions indicated.

moving with the same convection velocity as the Λ-vortex. Figure 8(*a*) shows the interpretation of figures 6(*c*, *d*). From figure 8 it can be seen that the Λ-vortex is lifting material up away from the surface. Material is brought down towards the wall at the sides and at the downstream end of the Λ-vortex. An interesting point is that the focus in figure 8(*a*), 'in the large', is 'unstable', i.e. material is spiralling out. However, closer to the focus, material should be spiralling in, since the vortex rod is being stretched. This latter aspect cannot be calculated, since the rod is being simulated by a line vortex of zero diameter. The spiralling out of material is necessary for continuity. It should be remembered that the pattern is unsteady, that this focus is moving out relative to the observer, and that the instantaneous streamlines cannot be interpreted as path lines or streaklines. Nevertheless, one can see that any material that finds its way into the instantaneous alleyway, shown shaded in figure 8(*b*), will be lifted from the surface. Figures 7(*a*, *b*) are typical of other planes parallel to the (x, y)-plane, and because of the 'stable' focus, i.e. because material is spiralling in,

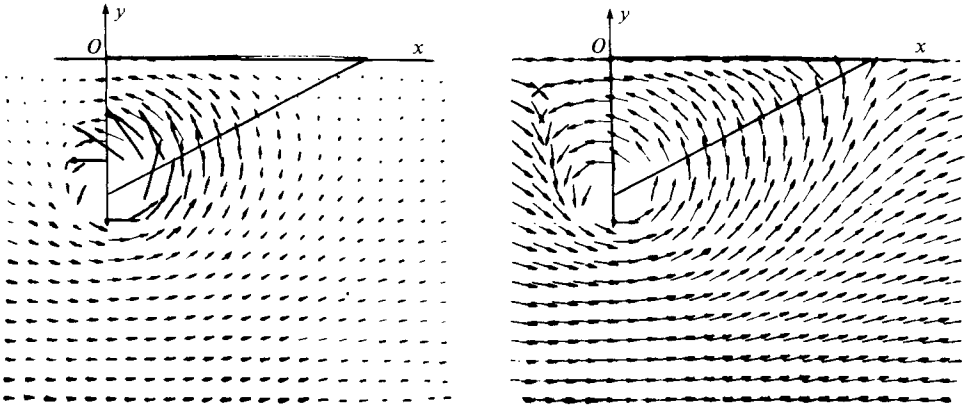

FIGURE 7. Velocity field on the (x, y)-plane of Λ-vortex as seen by an observer moving with the convection velocity of the vortex. (*a*) Velocity field. (*b*) Velocity directions only.

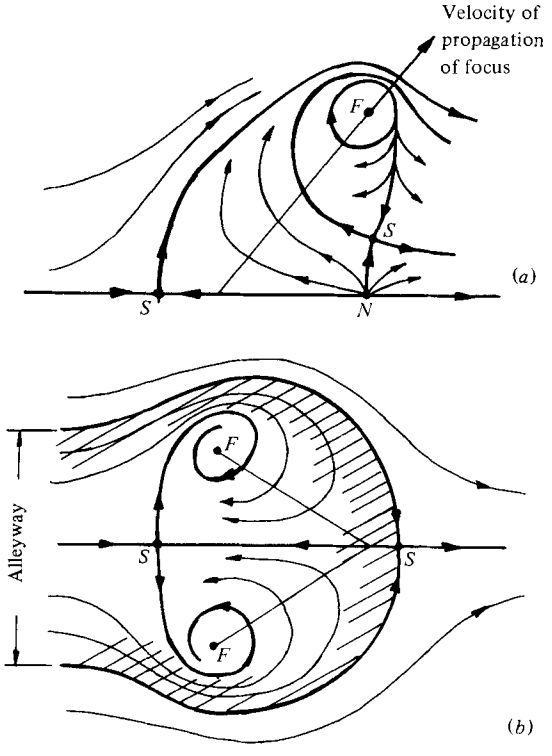

FIGURE 8. (*a*) Interpretation of figure 6(*d*). (*b*) Interpretation of figure 7(*b*).
S = saddle, F = focus, N = node.

it can be seen then that the rods are undergoing something like axisymmetrical strain. Thus, in the large, the Λ-vortex is undergoing approximately a plane-strain-like motion and the rods are undergoing locally, axisymmetrical strain. The discussion given earlier regarding the diffusion of vorticity and heat can therefore be applied to the rods. The plane-strain behaviour appears to occur in the ciné observations of trip-wire vortices by Perry *et al.* (1981).

4. A simple model for wall turbulence

4.1. *Analysis for mean vorticity and temperature-gradient distribution*

For simplicity, assume that all eddies are leaning in the downstream direction at a constant angle ϕ as shown in figure 9. Imagine we have a sampling volume $ABCD$, E units long, and slanting at the slope of the eddies. Let the cross-stream width of our sampling volume be λ_k, the average lateral spacing of the eddies.

We are going to derive an expression for the distribution of mean vorticity and mean-temperature gradient along the slanting line S as a function of z, the vertical distance from the wall. It will be assumed that over the finite distance E there is no significant variation in statistical quantities. Let a large number of randomly chosen realizations m be carried out within this sampling volume, each realization corresponding to a fixed instant of time. Let $L = mE$ and let all the eddies sampled be arranged in order of height h and distributed at a uniform spacing along this hypothetical sampling length L. This will give us a distribution of eddy heights as shown in figure 10. These heights are shown as vertical bars.

From the geometry and symmetry of the eddies, the mean vorticity produced by a random array of such eddies must be in the cross-stream direction. Hence we need only consider the y-component of vorticity. Again, it will be emphasized that all the vorticity in the flow resides in the rods and the surrounding fluid is irrotational.

The contribution to the mean vorticity $\overline{\eta}$ at level z above the surface will therefore depend on the number of rods of vorticity being cut. For the interval $\delta x'$ in figure 10 the elemental contribution is

$$\delta\overline{\eta} = \frac{2\eta_R A_R N_e \delta x'}{\lambda_k L}, \tag{4.1}$$

where x' is a distance measured along the hypothetical sampling length L, A_R is the cross-sectional area of the rod in the (x, y)-plane at level z, η_R is the average y-component of vorticity in the area A_R, and N_e is the number of eddies per unit length when spread uniformly over the length L. It is assumed that the average spacing of the eddies is independent of height. The factor of 2 is included since there are two legs to the Λ-vortex. For large m, (4.1) would give

$$\overline{\eta} = \int_{x_0'}^{L} \frac{2\eta_R A_R N_e}{\lambda_k L} dx'. \tag{4.2}$$

However, $x'/L = f_E(h/\delta)$, where δ is the height of the highest eddy. Changing the variable of integration gives

$$\frac{d\overline{U}_1}{dz} = \overline{\eta} = \int_z^{\delta} \frac{2\eta_R A_R N_e}{\lambda_k} \left\{\frac{1}{\delta} f_E'\left(\frac{h}{\delta}\right)\right\} dh, \tag{4.3}$$

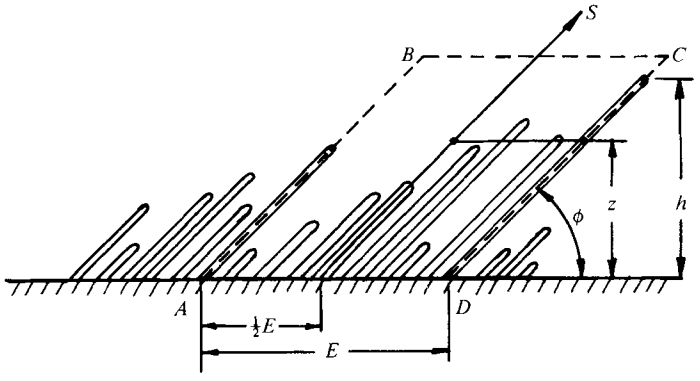

FIGURE 9. Random array of eddies and the sampling volume *ABCD*.

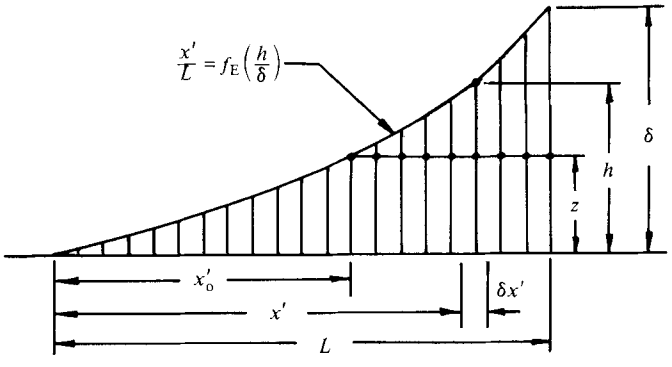

FIGURE 10. Arrangement of eddies in order of height.

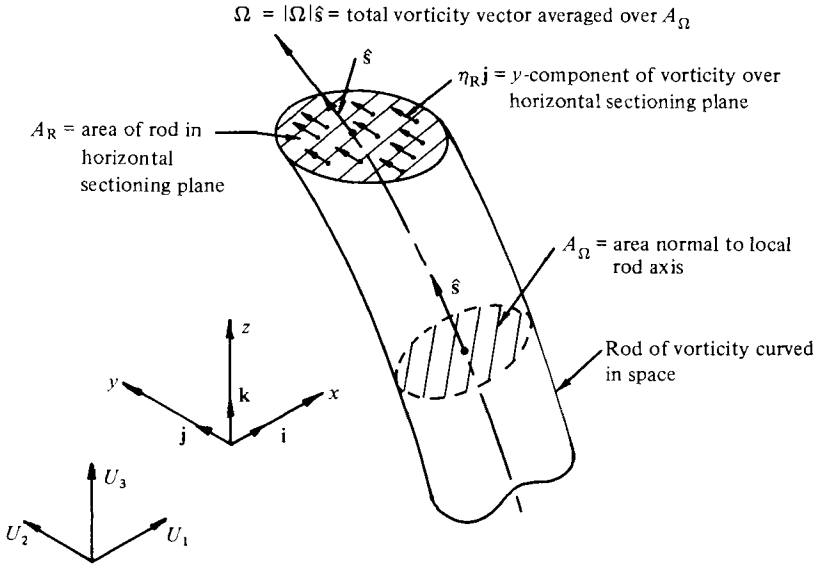

FIGURE 11. Rod of vorticity curved in space.

where $\overline{U}_1$ is the mean velocity in the x-direction. The quantity $\delta^{-1}f'_{\mathrm{E}}(h/\delta)$ is the normalized probability density function (p.d.f.) of eddy height h, i.e. $p_{\mathrm{E}}(h)$, and is normalized such that $\int_0^\infty p_{\mathrm{E}}(h)\,dh = 1$.

Considering for the moment that the rods are of uniform cross-sectional area along their length, but curved in space, figure 11 defines some of the various quantities, and A_Ω is the area of the rod normal to its local axis. It is simple to show that (4.3) can be written as

$$\frac{d\overline{U}_1}{dz} = \int_z^\delta \frac{2\hat{\mathbf{s}}.\mathbf{j}}{\hat{\mathbf{s}}.\mathbf{k}} \frac{|\boldsymbol{\Omega}|\,A_\Omega}{\lambda_k e} p_{\mathrm{E}}(h)\,dh, \tag{4.4}$$

where $e = 1/N_{\mathrm{e}}$ is the average streamwise spacing of the eddies. The x, y and z velocity components are respectively U_1, U_2 and U_3 in figure 11.

As mentioned in § 1, when eddies die by viscous diffusion and vorticity cancellation, the flow field surrounding the Λ-vortex is made up of debris which is assumed to be irrotational. However, heat that is carried away from the wall within the rods does not cancel, and so the hot rods will be surrounded by a background temperature of 'lukewarm' fluid resulting from this debris. Assuming that this background temperature is uniform, an analysis similar to that carried out for the mean vorticity leads to

$$\frac{d\overline{\theta}}{dz} = \frac{d}{dz}\int_z^\delta \frac{2\theta'_{\mathrm{R}} A_\theta}{\hat{\mathbf{s}}.\mathbf{k}\lambda_k e} p_{\mathrm{E}}(h)\,dh. \tag{4.5}$$

Let θ denote temperatures measured relative to the wall, and define $\theta_j = T_{\mathrm{w}} - T_j$; let the suffix w denote wall. The suffix j can be replaced by R, meaning rod, or b, meaning background temperature. θ is the mean fluid temperature relative to the wall, and $\theta'_{\mathrm{R}} = \theta_{\mathrm{R}} - \theta_{\mathrm{b}}$. It is convenient to measure the rod temperature relative to the background temperature so that the weighting factors in the integral (4.5) are the same as those in (4.4).

A general curved Λ-vortex (which has a plane of symmetry) can be described by two equations:

$$\frac{x}{h} = F\left(\frac{z}{h}, \frac{h}{l}\right), \quad \frac{y}{\lambda} = G\left(\frac{z}{\lambda}, \frac{\lambda}{h}\right), \tag{4.6}$$

where l is an extra length scale yet to be defined. As the vortex is stretched, two conservation principles have to be observed. These are the conservation of circulation and heat:

$$|\boldsymbol{\Omega}|A_\Omega = |\boldsymbol{\Omega}_0|A_{\Omega_0}, \tag{4.7}$$

$$\theta'_{\mathrm{R}} A_\theta C = \theta'_{\mathrm{R}_0} A_{\theta_0} C_0, \tag{4.8}$$

where the subscript 0 denotes initial values, say when the vortex has completed its roll-up, and C is the arc length of the rod.

From (4.4)–(4.8), it can be shown after a considerable amount of algebra that

$$\frac{d\overline{U}_1}{dz} = \int_z^\delta \frac{2G'|\boldsymbol{\Omega}_0|A_{\Omega_0}}{\lambda_k e} p_{\mathrm{E}}(h)\,dh, \tag{4.9}$$

$$\frac{d\overline{\theta}}{dz} = \frac{d}{dz}\int_z^\delta \frac{\theta'_{\mathrm{R}_0} A_{\theta_0} C_0 (F'^2 + G'^2 + 1)^{\frac{1}{2}}}{\lambda_k e h \int_0^1 (F'^2 + G'^2 + 1)^{\frac{1}{2}}\,d(z/h)} p_{\mathrm{E}}(h)\,dh, \tag{4.10}$$

where $F' = dF/d(z/h)$ and $G' = dG/d(z/\lambda)$.

The crude calculation given in § 3, where the rods were assumed to be straight, indicated that the growth rate of the vortices is uniform, implying a linear distribution of eddy heights in figure 10. This would give a flat p.d.f. with $p_{\mathrm{E}}(h) = 1/\delta$ in the interval $0 < h < \delta$, and zero elsewhere. We are now seeking solutions such that $d\overline{U}_1/dz \sim z^{-1}$ and $d\overline{\theta}/dz \sim z^{-1}$ for z/δ small,† treating δ as an outer length scale of the boundary layer. This is to satisfy the results given in table 1.

The only way to produce the correct result for temperature is to have straight rods giving

$$(F'^2 + G'^2 + 1)^{\frac{1}{2}} = \int_0^1 (F'^2 + G'^2 + 1)^{\frac{1}{2}} d(z/h),$$

since F'^2 and G'^2 are constants. Hence

$$\frac{d\overline{\theta}}{dz} = -\frac{\theta'_{\mathrm{R}_0} A_{\theta_0} C_0}{\lambda_k e \delta} \frac{1}{z}. \tag{4.11}$$

The rod angle ϕ can be a function of h, but the rods must be straight. Since the rods are straight, and, if we continue with the assumption that the angle ϕ is constant, then the extra length scale l in (4.6) is not needed, as this is associated with the projected slope of the vortex in the (x, z)-plane.

To obtain the correct variation for the vorticity, plane strain must occur in the (y, z)-projection of the eddy. G' is then given by $G' = \lambda_0 h_0 / 2h^2$, and so

$$\frac{d\overline{U}_1}{dz} = \frac{\lambda_0 h_0 |\boldsymbol{\Omega}_0| A_{\Omega_0}}{\lambda_k e \delta} \left\{ \frac{1}{z} - \frac{1}{\delta} \right\}, \tag{4.12}$$

which gives the required result for $z \ll \delta$. The quantities λ_0 and h_0 could be regarded as the initial values of λ and h just after the vortex has completed its roll-up and plane strain has just commenced.

4.2. *Eddy 'generations'*

We see that with (4.12) there is an immediate difficulty. If we wish to take δ to arbitrary large values then $d\overline{U}_1/dz \to 0$ as $\delta \to \infty$ at finite z. This odd behaviour is due to the fact that we have not taken into account that there exists a population problem, which can be explained best by an example. Figure 12 (*a*) shows an orderly array of Λ-vortices produced periodically from a source O. One can see that the range of eddy heights sampled in the measuring volume is limited. Even if the source at O is jittered back and forth along the x-axis, the sampling will still be limited. Figure 12 (*b*) shows a more-realistic picture where there are a number of sources O, O', O''. We imagine that each time an eddy reaches a height δ_0 a new 'generation' of eddies is 'born' at the wall. With jitter, our measuring volume will sample all scales of eddies.

Consider a flow in a pipe. Here conditions are statistically uniform with streamwise distance x, so we can make our measuring volume any size. Suppose that we make it p, as defined in figure 12 (*b*) and that there are n generations of eddies. In one realization all eddy sizes have been sampled for the ideal case illustrated, and, when the eddies are stacked in order of size, a linear distribution would result for figure 10.

It can be seen that $\delta = n\delta_0$, where n is the number of generations, and, as $\delta \to \infty$, $n \to \infty$. (Also n need not be an integer.) The important feature shown in the diagrams is that the spacing of the eddies diminishes as n increases. In fact, as δ grows we have

† Throughout this paper $\sim$ means 'proportional to' or 'scales with'.

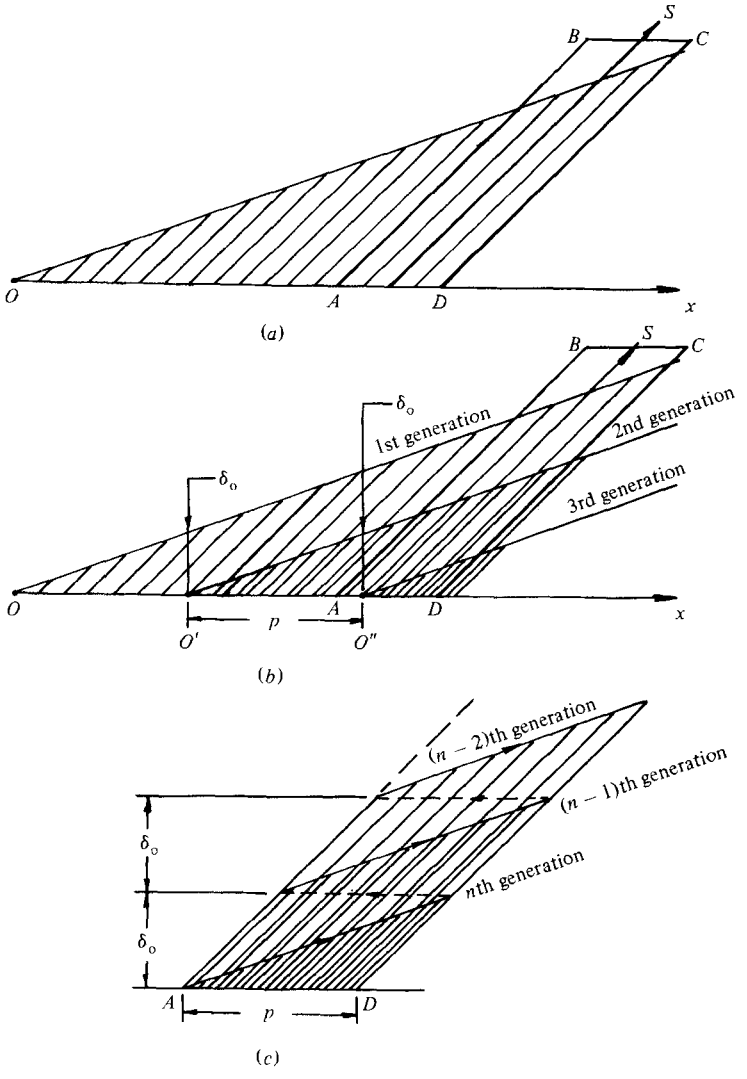

FIGURE 12. Eddy generations (see text).

a 'population explosion' at the wall. Thus e in equation (4.12) should be replaced by e/n, and e is now interpreted as the average spacing of eddies in a given generation. The quantity δ is replaced by $n\delta_0$, and so (4.12) becomes

$$\frac{d\overline{U}_1}{dz} = \frac{\lambda_0 h_0 |\boldsymbol{\Omega}_0| A_{\Omega_0}}{\lambda_k e \delta_0} \left\{\frac{1}{z} - \frac{1}{\delta}\right\}. \tag{4.13}$$

In the limit of $\delta \to \infty$, the equation has the correct behaviour. The population density increase is not important close to the wall, since the eddies with larger height h make diminishing contributions to the mean vorticity.

4.3. *Scaling of the eddies*

On the completion of vortex roll-up of the disturbed sublayer material, a Kline scaling will be assumed (see Kline *et al.* 1967; Head & Bandyopadhyay 1981). We will assume that all length scales at roll-up scale with ν/U_τ, including the length of vortex sheet l_a that is rolled up to form the rods (see figure 13*a*).

Let $\lambda_0 = a_1\nu/U_\tau, h_0 = b_1\nu/U_\tau$, the characteristic velocity jump across the sheet $\Delta U = c_1 U_\tau$, $l_a = d_1\nu/U_\tau$, $e = e_1\nu/U_\tau$, $\lambda_k = f_1\nu/U_\tau$, $\delta_0 = g_1\nu/U_\tau$ and $\epsilon = h_1\nu/U_\tau$. Therefore $|\boldsymbol{\Omega}_0|A_{\Omega_0} = \Delta U l_a = c_1 d_1 \nu$. Substituting all of these into (4.13) gives the classical result for $z \ll \delta$, i.e.

$$\frac{d\overline{U}_1}{dz} = \frac{U_\tau}{\kappa z}, \tag{4.14}$$

where

$$\kappa = \frac{f_1 e_1 g_1}{a_1 b_1 c_1 d_1}$$

is the von Kármán universal mixing constant.

A rough order-of-magnitude check can be made by substituting into (4.14) some reasonable 'guesses' for the various constants. If we imagine that a 'carpet' of cross-stream vorticity U_τ^2/ν, e units long and $5\nu/U_\tau$ units thick (the thickness of a viscous sublayer), is distorted and wrapped into two rods of vorticity as shown in figure 13(*b*), then $\Delta U l_a = A_{\Omega_0}|\boldsymbol{\Omega}_0| = 5e_1\nu$, and so $c_1 d_1 = 5e_1$. Taking $f_1 = 100$, $e_1 = 200$, $g_1 = 100$, $a_1 = 100$ and $b_1 = 50$ gives $\kappa = 0{\cdot}4$, which is close to the accepted value.

A similar analysis can be carried out for the temperature distribution if we assume that $-\theta'_{R_0}$ scales with the friction temperature θ_τ where $\theta_\tau = q_0/\rho C_p U_\tau$, where q_0 is the heat flux, ρ is the fluid density and C_p is the specific heat. Furthermore, for fluids with a Prandtl number of unity or higher (gases to oils) A_{θ_0} will be approximately equal to A_{Ω_0}. Hence put $-\theta'_{R_0} = k_1\theta_\tau$, $A_{\theta_0} = \epsilon l_a = h_1 d_1(\nu/U_\tau)^2$, $C_0 = l_1\nu/U_\tau$. Substitution into (4.11) gives the classical result

$$\frac{d\overline{\theta}}{dz} = \frac{\theta_\tau}{\kappa_H z}, \tag{4.15}$$

where

$$\kappa_H = \frac{f_1 e_1 g_1}{k_1 h_1 d_1 l_1}$$

is the thermal analogue of κ.

For a fully rough surface (i.e. when we are in the rough regime) we will define a roughness scale k such that $\lambda_k = f_1 k$. This follows a suggestion by Grass (1971). It will be assumed that all large-scale features of the vortex produced at the completion of roll-up are geometrically similar to that from a smooth surface, but have a length scale k, and that the characteristic velocity scale will be U_τ in both cases, since this is related to the wall shear stress. Fine-scale features such as the thickness of the sheet will involve viscosity, and this will not fit in with the similarity scheme. However, we would expect $e = e_1 k$, $\delta_0 = g_1 k$, $\lambda_0 = a_1 k$, $h_0 = b_1 k$, $\Delta U = c_1 U_\tau$, $l_a = d_1 k$, and hence $|\boldsymbol{\Omega}_0|A_{\Omega_0} = c_1 d_1 k U_\tau$. Substitution into (4.13) gives (4.14) as before.

An interesting point to note is that the effects of viscous and thermal diffusion have been accounted for in the analysis by using the conservation laws (4.7) and (4.8), i.e. viscous and thermal diffusion takes place during the plane-strain process, and yet the classical results are obtained which are independent of ν and the thermal diffusivity coefficient. This satisfies the Townsend (1976) Reynolds-number similarity hypothesis.

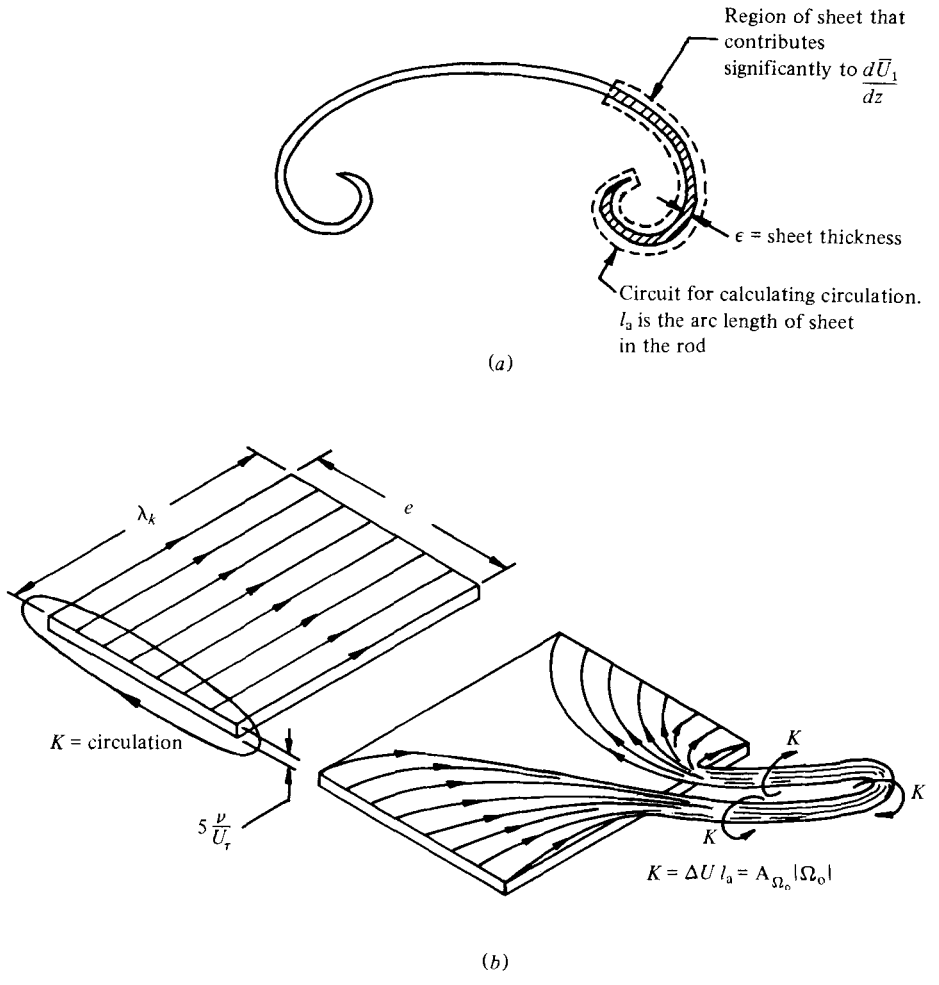

FIGURE 13. (*a*) Cross-section of eddy. (*b*) Carpet of vorticity being wrapped into vortex (schematic).

4.4. *Death of eddies and the necessity for hierarchies*

The classical results (given by (4.14) and (4.15)) have been succesfully derived with plausible assumptions, and are consistent with the Biot–Savart law. Unfortunately, as the Λ-vortex is stretched more and more under plane strain, the legs approach each other and viscous diffusion must ultimately dominate over this uniform stretching, as shown by (2.9). Vorticity cancellation must cause the eddy to 'die'. Even prior to this cancellation process, the eddy is of no consequence regarding the mean-flow field close to the wall, since its contribution to the mean vorticity becomes progressively weaker as its h/λ ratio becomes progressively higher. In fact, using (2.9) one can deduce, if $V\,(=dh/dt)$ scales with U_τ, that the eddy 'death' must commence at a fixed value of $h_+\,(=hU_\tau/\nu)$. However, it has always been accepted that the logarithmic law of the wall (given by (4.14)) is valid for arbitrary large values of z_+ for $\delta U_\tau/\nu \to \infty$. Hence the model presented so far, attractive though it may be, is incomplete, and is not the only model that fits the 'facts'.

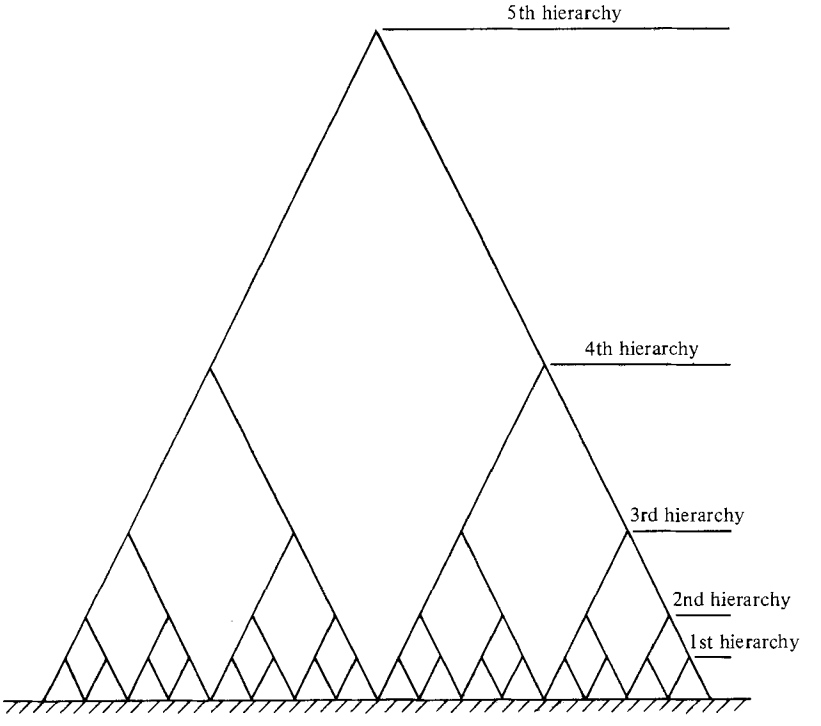

FIGURE 14. Symbolic representation of a discrete system of hierarchies.

5. Hierarchies of eddies

5.1. *Introduction*

In order to extend the law of the wall we have to introduce hierarchies of eddies that are geometrically similar and there are many ways of doing this.

To preserve the Kline streaks at the wall, which scale according to $\lambda_k = 100\nu/U_\tau$, a series of geometrically similar hierarchies could be stacked according to figure 14, where the scales of the hierarchies are in a geometrical progression. Within each hierarchy, plane strain is occurring and the eddies grow from their initial roll-up height to a height δ, where δ is the height of the highest eddy within the hierarchy. The number of hierarchies will increase with Reynolds number, but the structures become finer within a given hierarchy with decreasing ν/U_τ. Some evidence for this can be seen in Head & Bandyopadhyay (1981, figure 32, plate 9).

Although, for low values of z/δ in a given hierarchy, contributions to the mean vorticity by eddies of height $h/\delta \to 1$ may be unimportant, this is not true for $z/\delta \to 1$. Now that we have hierarchies of eddies, z/δ can be arbitrarily large even though z/Δ_E may be small. Here Δ_E is the true boundary-layer thickness, which is the height of the highest eddy in the highest hierarchy. Now, in a given hierarchy, δ will be limited, and will be defined as the height at which the legs of the Λ-vortex begin to merge. Any eddies higher than δ are assumed to be of no consequence. It is conjectured that δ is limited and that only the first two or three 'youngest' generations have any significant effect. The original equation (4.12) will now be used, where it is understood that e is the average spacing of eddies in a hierarchy (and not in a given generation)

and that δ is limited. In the first hierarchy, it will again be assumed that viscous scaling is valid and that δ scales with ν/U_τ.

It will be assumed that all length scales double as we go from one hierarchy to the next. However, since all hierarchies are made from the same sublayer material, the characteristic sheet strength or velocity jump ΔU is the same and scales with U_τ. In the first hierarchy, all quantities are as before except $e = e_2\nu/U_\tau$ and $\delta = g_2\nu/U_\tau$, giving $\kappa = f_1e_2g_2/a_1b_1c_1d_1$, which is the same as the previous κ, since, although the definition of e is different and δ replaces δ_0, the product e_2g_2 equals e_1g_1. Now, for consecutive hierarchies, λ_0, h_0, λ_k, e and δ will double. So also will $|\boldsymbol{\Omega}_0|A_{\Omega_0}$, since this is given by $|\boldsymbol{\Omega}_0|A_{\Omega_0} = \Delta U l_a$, and l_a will double. There are two ways of looking at this. We could consider $A_{\Omega_0} \sim \delta$ and $|\boldsymbol{\Omega}_0|$ fixed, or alternatively the 'smeared-out area' of the rod $A_{\Omega_0} \sim \delta^2$ and the smeared-out $|\boldsymbol{\Omega}_0| \sim 1/\delta$. In either case, the circulation doubles, giving many groups of geometrically similar eddies which have the same characteristic velocity scale. It will be seen later that this is consistent with the Townsend attached-eddy hypothesis, and is one necessary condition for giving constant Reynolds shear stress. Hence, each hierarchy of eddies gives

$$\frac{d\overline{U}_1}{dz} = \frac{U_\tau}{\kappa}\left\{\frac{1}{z} - \frac{1}{\delta}\right\}, \tag{5.1}$$

and if δ_1 is the scale of the first hierarchy

$$\frac{d\overline{U}_1}{dz} = \sum_{n=1}^{N} \frac{U_\tau}{\kappa}\left\{\frac{1}{z} - \frac{1}{2^{n-1}\delta_1}\right\}, \tag{5.2}$$

where N is the number of hierarchies. As $N \to \infty$, i.e. as $\Delta_E = \delta_1 2^{N-1} \to \infty$, $d\overline{U}_1/dz$ does not converge. We have been assuming that all hierarchies have small h_0 and that plane strain effectively starts at the wall with the appropriate lateral length scale, and this may not be correct. Hence it is necessary to consider how the hierarchies are formed.

5.2. *The 'quantum-jump' or discrete system of eddies*

One way to make the model work is to assume that all hierarchies other than the first have no eddy heights less than $b\delta$, where δ is the scale of the hierarchy under consideration. It will be seen later that b must equal $\frac{1}{2}$. Thus, in each hierarchy, the shortest eddy which is to undergo plane strain must appear from 'nowhere'. Vortex pairing of two eddies in one hierarchy to form an eddy for the next hierarchy is one possible explanation. Two eddies which are of the largest height in a given hierarchy pair to give the shortest eddy for the next hierarchy. In fact one must assume that half the eddies in a given hierarchy are destined to pair and the other half are destined to die. Suppose we go back to our sampling volume and count only those eddies in a given hierarchy which have geometrically similar 'partners' in other hierarchies. All eddies can be stacked in order of size as before and we obtain the distribution given in figure 15. We now repeat the analysis given in § 4.1 for each hierarchy, and this gives

$$\frac{d\overline{U}_1}{dz} = \frac{\lambda_0 h_0 |\boldsymbol{\Omega}_0| A_{\Omega_0}}{\lambda_k e(1-b)\delta}\left\{\frac{1}{z} - \frac{1}{\delta}\right\}, \tag{5.3}$$

where e is now the average spacing between eddies that have geometrically similar partners in other hierarchies. This may be written again as (5.1) with the same κ.†

† This is because the definition of e has changed so that the final value of κ again remains unaffected.

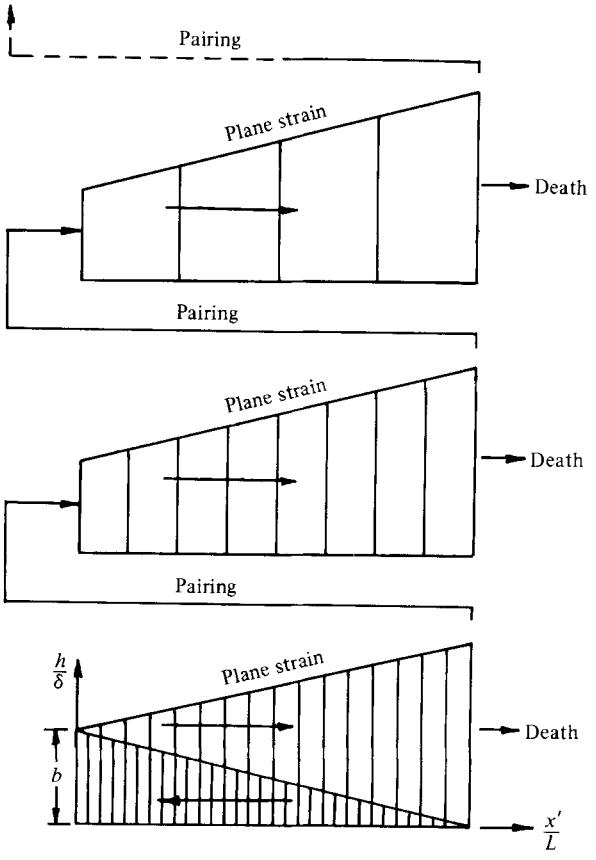

FIGURE 15. 'Quantum-jump' or vortex-pairing model.

It should be noted that, in the first hierarchy, extra non-geometrically similar eddies have been added and 'folded back' in figure 15 to simulate the fact that eddies undergo plane strain from the wall for this hierarchy.

For the first hierarchy and with $b = \frac{1}{2}$, $d\overline{U}_1/dz$ is given by

$$\frac{d\overline{U}_1}{dz} = \frac{U_\tau}{\kappa}\left\{\frac{1}{z} - \frac{1}{\delta_1}\right\}[1 - H(z - \delta_1)],$$

where H is a Heaviside function. For subsequent hierarchies

$$\frac{d\overline{U}_1}{dz} = \frac{U_\tau}{\kappa}\left\{\frac{1}{\delta}[1 - H(z - \tfrac{1}{2}\delta)] + \left(\frac{1}{z} - \frac{1}{\delta}\right)[H(z - \tfrac{1}{2}\delta) - H(z - \delta)]\right\}.$$

The reason for the flat distribution of vorticity between $0 < z < \frac{1}{2}\delta$ in the above equation is that the number of eddies being cut remains constant for $z < \frac{1}{2}\delta$. The complete distribution is therefore given by

$$\frac{d\overline{U}_1}{dz} = \frac{U_\tau}{\kappa}\left[\frac{1}{z} - \frac{1}{\delta_1}\right][1 - H(z - \delta_1)] + \sum_{n=2}^{N}\frac{U_\tau}{\kappa}\left\{\frac{1}{\delta_1 2^{n-1}}[1 - H(z - \delta_1 2^{n-2})]\right.$$
$$\left. + \left[\frac{1}{z} - \frac{1}{\delta_1 2^{n-1}}\right][H(z - \delta_1 2^{n-2}) - H(z - \delta_1 2^{n-1})]\right\},$$

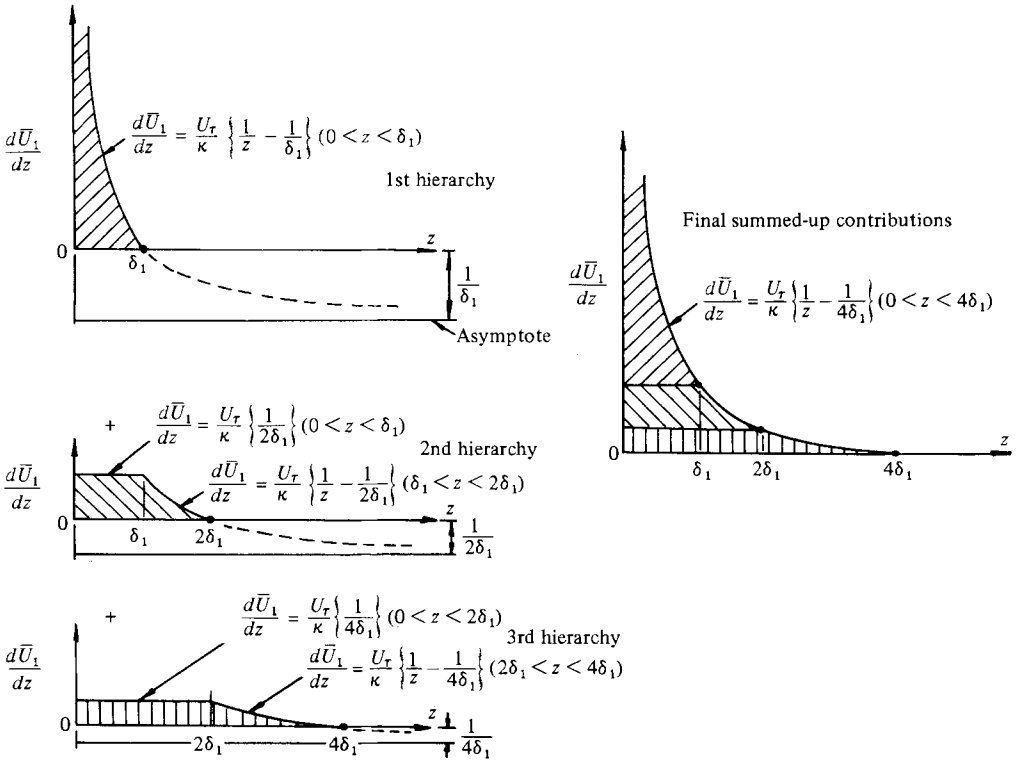

FIGURE 16. How profiles are summed up for three hierarchies. Relationships are shown without Heaviside functions.

which reduces to the amazingly simple result that

$$\frac{d\bar{U}_1}{dz} = \frac{U_\tau}{\kappa}\left\{\frac{1}{z} - \frac{1}{\Delta_E}\right\}, \tag{5.4}$$

with $\Delta_E = 2^{N-1}\delta_1$. This is best understood from a graphical construction as shown in figure 16. If $b > \frac{1}{2}$, 'plateaus' will appear and, for $b < \frac{1}{2}$, 'bumps' due to overlapping will occur in the final velocity distribution.

The idea of vortex pairing is consistent with the scaling laws developed earlier. The circulation doubles if the length scale of the hierarchy doubles. Vortex pairing may not be the only mechanism, and this is discussed in §5.4.

To simulate the possibility that eddies at the wall take time to roll up, and therefore their growth rate is initially slower, further weighting can be put into the distributions, as shown in figure 17, and could be adjusted to give the well-known buffer zone. The normalized p.d.f. $p_E(h)$ used in §4.1 turns out to be proportional to $\tan\psi$, i.e.

$$p_E(h) = \frac{1}{\delta} f'_E(h/\delta) = \frac{1}{\delta}\tan\psi = \frac{1}{(1-b)\,\delta}.$$

This gives the distribution of eddies that have geometrically similar partners in other hierarchies, and is normalized to unit area because of the definition of e (the spacing of such eddies). The extra weighting is shown in figure 17(a, b), and the viscous sublayer could be simulated by something approaching a Dirac delta function. The

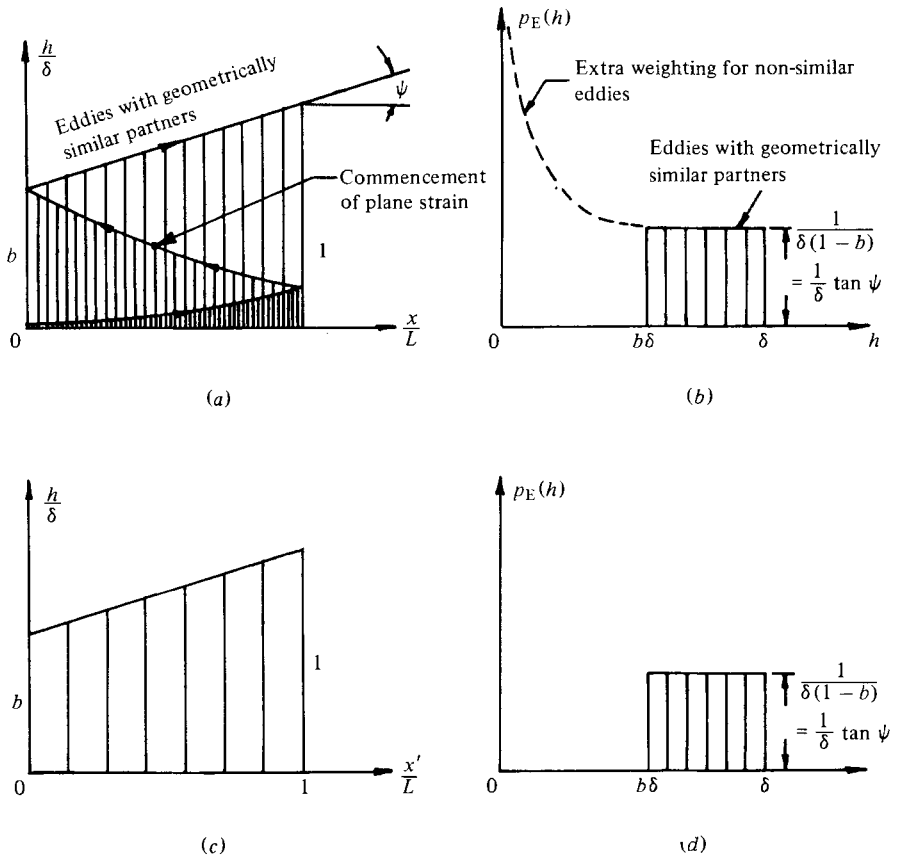

FIGURE 17. Arrangement of eddies and associated p.d.f.s. (*a*) First hierarchy; (*b*) associated p.d.f. (*c*) Hierarchies higher than the first; (*d*) associated p.d.f.

resulting 'law of the wall' is shown in figure 18. It should be remembered that δ_1 scales with ν/U_τ.

This pairing process, if it exists, would give the eddy a new 'lease of life', since, 'in the large', its scale is growing uniformly with time, whereas, with viscous diffusion, its scale varies with $(\nu t)^{\frac{1}{2}}$. Thus the inviscid process of pairing will dominate. However, if an eddy is 'unlucky' and does not find a 'partner', it will die by viscous diffusion and vorticity cancellation.

5.3. *Temperature distribution with hierarchies*

A similar analysis can be carried out for temperature. However, a problem occurs when considering the definition of $1/\kappa_H$, which from (4.11) is

$$\frac{\theta_\tau}{\kappa_H} = \frac{-\theta'_{R_0} A_{\theta_0} C_0}{\lambda_k e \delta}. \tag{5.5}$$

The higher hierarchies are made from the same sublayer material, so $-\theta'_{R_0} = k_1 \theta_\tau$ as before, but A_{θ_0} scales with δ. In effect, the heat content of the rod doubles as the scale of the eddy doubles. Since C_0, λ_k and e will all scale with δ, $1/\kappa_H$ will scale with $1/\delta$. Thus the mixing constant for the thermal law of the wall halves from one hierarchy

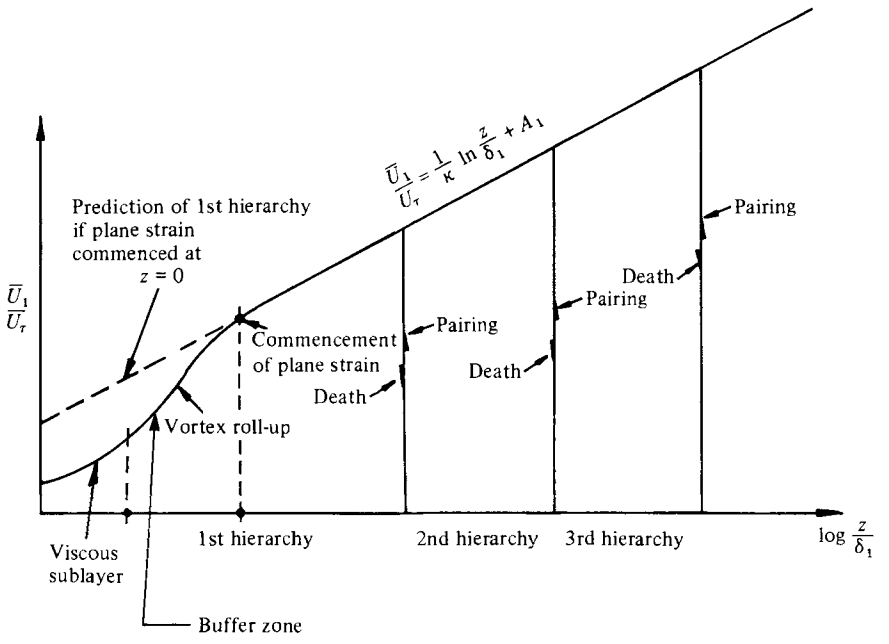

FIGURE 18. Mean-velocity profile interpreted in terms of quantum-jump model. A_1 is a universal constant.

to the next. There are two reasons why the temperature profile will not do this but will actually tend to follow a constant $1/\kappa_H$. The first reason is that $-\theta'_{R_0}$ is the rod temperature measured relative to the background temperature θ_b. Since we have hierarchies, the debris deposited by each hierarchy on eddy death will set up a gradient in the background temperature. The second reason is that this background temperature will be very high close to the boundary, and material entrained into the rods will be transported within the rods from the lower hotter regions to the higher cooler regions, causing A_{θ_0} to scale between δ and δ^2. The transport of heat in the surrounding irrotational fluid would have to be computed, and this is analytically intractable.

The strong mixing of the irrotational motions close to the wall and the high concentration of debris is evident from the very 'foggy' appearance of the smoke close to the boundary. The authors have observed this, and so also have Head & Bandyopadhyay. Realizing that smoke has a very high Schmidt number, these mixing processes must be very strong, and make it extremely difficult to observe the formation of eddies at the boundary because of a lack of an air–smoke interface. These new eddies can be seen only after the smoke is introduced well downstream of the boundary-layer origin (see Head & Bandyopadhyay 1981).

5.4. *Discrete system and distributed system of hierarchies*

So far we have considered a system of hierarchies whose length scale goes in geometrical progression with a factor of 2 from one hierarchy to the next. When randomness is introduced into the process, this quantum-jump phenomenon could well be smoothed out. With jitter in the various quantities, the net result could perhaps be better described by a continuous distribution of scales. In fact, certain other mechanisms suggest themselves with this continuous distribution.

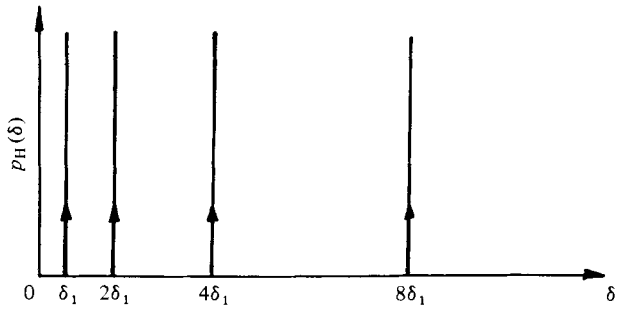

(a)

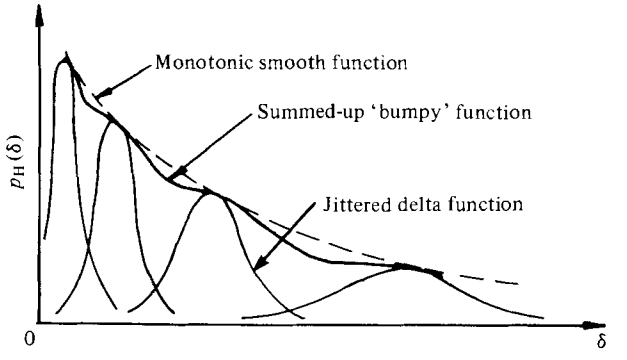

(b)

FIGURE 19. Hierarchy p.d.f.s. (a) Discrete distribution. (b) Continuous distribution resulting from jitter.

With the model so far, for $z > b\delta_1$, what we are effectively doing is to say that, if $d\overline{U}_1/dz$ for each hierarchy is written as $f(z, \delta)$, then the resulting distribution of $d\overline{U}_1/dz$ is given by

$$\frac{d\overline{U}_1}{dz} = \sum_{n=1}^{N} f(z, \delta_1 2^{n-1}), \tag{5.6}$$

where δ_1 is the smallest hierarchy scale. Equation (5.6) could be written as

$$\frac{d\overline{U}_1}{dz} = \int_{\delta_1}^{\Delta_E} f(z, \delta) p_H(\delta)\, d\delta, \tag{5.7}$$

where $p_H(\delta)$ is the probability distribution for hierarchy scales. For the special case of (5.6), $p_H(\delta)$ is a series of unit delta functions as shown in figure 19(a). With random jitter, this will lead to the 'bumpy' function shown in figure 19(b). It is shown in appendix A that a truly monotonic distribution that preserves the 'geometrical progression' property of our original distribution is

$$p_E(\delta) = \frac{M}{\delta}, \tag{5.8}$$

where M is a constant of order unity. Thus

$$\sum_{n=1}^{N} f(z, \delta_1 2^{n-1}) \nsim \int_{\delta_1}^{\Delta_E} f(z, \delta) \frac{M}{\delta} d\delta, \tag{5.9}$$

where the symbol $\stackrel{\wedge}{=}$ means that the right-hand side is the distributed analogue of the discrete left-hand side.

5.5. *Mean vorticity with a distributed system of hierarchies*

The mean vorticity is now derived for a continuous distribution of hierarchies thus:

$$\frac{d\bar{U}_1}{dz} = \int_{\delta_1}^{\Delta_E} f(z,\delta)\frac{M}{\delta}\,d\delta, \tag{5.10}$$

where again δ_1 is the smallest hierarchy. The function f is obtained by assuming the distribution of eddies as given in figure 17. To simulate the possibility that, as the hierarchy scale grows, fewer and fewer hierarchies are formed at the wall, but originate from a pairing process as the hierarchy scale δ increases, the degree of foldback shown earlier could be made a function of δ and should diminish with increasing hierarchy scale. This would simulate the buffer zone. Suppose that $z > \delta_1$ is sufficiently far from the wall that we can ignore these foldbacks. The appropriate function $f(z,\delta)$ is then given by

$$f(z,\delta) = [1-H(z-b\delta)]\left\{\frac{U_\tau}{\kappa'}\left(\frac{1}{1-b}\right)\left(\frac{1}{b\delta}-\frac{1}{\delta}\right)\right\} + [H(z-b\delta)-H(z-\Delta_E)]\left\{\frac{U_\tau}{\kappa'}\left(\frac{1}{1-b}\right)\left(\frac{1}{z}-\frac{1}{\delta}\right)\right., \tag{5.11}$$

where κ' is the κ given earlier, but since new constants will appear the symbol κ will be reserved for the von Kármán mixing constant that finally emerges.

After performing the integration given by (5.10) we obtain a number of zones with analytical expressions, the only one of interest being $\delta_1 < z < b\Delta_E$, which is

$$\frac{d\bar{U}_1}{dz} = \frac{MU_\tau}{\kappa'}\left\{\frac{\ln(1/b)}{1-b}\frac{1}{z}-\frac{1}{b\Delta_E}\right\}. \tag{5.12}$$

This is the only region where the logarithmic law of the wall can occur. For b finite and for

$$\frac{z}{\Delta_E}\frac{1-b}{b\ln(1/b)} \ll 1,$$

(5.12) reduces to

$$\frac{d\bar{U}_1}{dz} = \frac{U_\tau}{\kappa}\frac{1}{z}, \tag{5.13}$$

where

$$\kappa = \frac{\kappa'}{M}\frac{1-b}{\ln(1/b)}.$$

If $b = 0$, this means effectively that all hierarchy scales originate from the wall with their appropriate lateral scale and undergo plane strain. Equation (5.12) then becomes

$$\frac{d\bar{U}_1}{dz} = \lim_{b\to 0}\left\{\frac{MU_\tau}{\kappa'}\left[\frac{1}{z}\ln\frac{1}{b}-\frac{1}{b\Delta_E}\right]\right\} = -\frac{MU_\tau}{\kappa' b\Delta_E}, \tag{5.14}$$

which will obviously not lead to a logarithmic profile. If $b \to 1$, then (5.12) will give

$$\frac{d\bar{U}_1}{dz} = \frac{U_\tau}{\kappa}\left\{\frac{1}{z}-\frac{1}{\Delta_E}\right\}, \tag{5.15}$$

where $\kappa = \kappa'/M$.

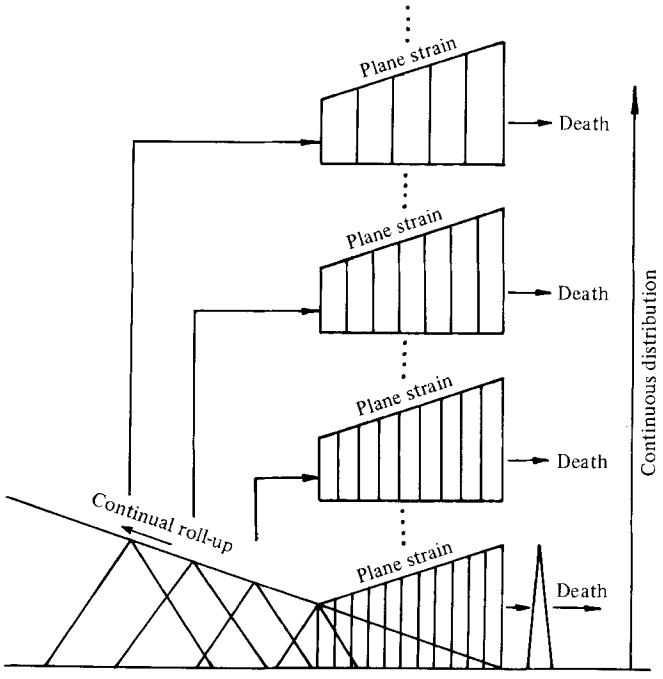

FIGURE 20. The continual roll-up and plane-strain model.

This case has no plane strain, and the eddies are continually growing, preserving their shape, and increasing their circulation K such that $K \sim \delta$. This would correspond to the Townsend attached-eddy model (Townsend 1976). Townsend did not apply this model to mean vorticity but to turbulent-energy distributions, but he did assume in effect that all eddies were geometrically similar, that the circulation grew with scale (to give a constant velocity scale), and that the probability distribution $p_{\mathrm{H}}(\delta)$ scales with $1/\delta$. An interesting point is that (5.15) is the same result obtained with plane strain but with only one hierarchy. This is also the result obtained with the discrete system with $b = \frac{1}{2}$ ((5.4)). With this model, the eddy is continually rolling up, but its likelihood of survival must diminish with scale so as to give the correct probability distribution.

This leads to the idea of another possible model – namely, a combination of both processes. We have eddies that are continually rolling up until somehow this process is disturbed and they then undergo plane strain and die. This would give a genuinely distributed system of eddy hierarchies where plane strain occurs in each hierarchy. This model avoids all hierarchies forming at the wall at their appropriate hierarchy scale. Rather, they all form at the wall with the Kline scaling. Vortex pairing is no longer needed. Figure 20 shows this sequence of events schematically.

With this model, (5.12) is applicable. Again, since the velocity scale of the eddy is constant during this roll-up stage, its growth is uniform in time. Thus this growth dominates over viscous diffusion. However, once the process of roll-up ceases and plane strain occurs, viscous diffusion must ultimately dominate, leading to eddy death.

6. Broad-band turbulence intensities and cross-correlations

Each eddy will have a velocity function

$$\frac{u_i}{U_0} = f_i\left(\frac{\mathbf{x}}{\delta}, \frac{h}{\delta}\right), \tag{6.1}$$

where u_i is the fluctuation about a mean. Of course, u_i cannot be computed from the Biot–Savart law unless we know the contributions of the eddies to the mean velocity $\overline{U}_1$, and this depends on the arrangement of the eddies. However, since $\overline{U}_2 = 0$ and $\overline{U}_3 = 0$, u_2 and u_3 can be readily computed using the Biot–Savart law. U_0 is the characteristic velocity scale of the eddy and h/δ is its 'strain number' (i.e. a measure of how much it has been stretched), and δ is the scale of the hierarchy. It is quite valid to use the same velocity scale U_0 for all eddies in a given hierarchy. It could be defined, for instance, as the induced value of u_i at some fixed standard value of $\mathbf{x}/\delta$ by an eddy of a fixed standard 'strain number' h/δ. If we double the scale of δ in moving from one hierarchy to another, then, according to the scaling laws given earlier, we must double the circulation. It is then simple to show that U_0 then remains fixed even from one hierarchy to the next.

If we are at a fixed value of z, the total contribution $\delta(u_i u_j)$ made by one isolated eddy is given by

$$\begin{aligned}\delta(u_i u_j) &= \iint_{-\infty}^{\infty} u_i u_j \, dx\, dy \\ &= U_0 \delta^2 \iint_{-\infty}^{\infty} f_i\left(\frac{\mathbf{x}}{\delta}, \frac{h}{\delta}\right) f_j\left(\frac{\mathbf{x}}{\delta}, \frac{h}{\delta}\right) d\left(\frac{x}{\delta}\right) d\left(\frac{y}{\delta}\right) \\ &= \delta^2 U_0^2 \phi_{ij}\left(\frac{z}{\delta}, \frac{h}{\delta}\right).\end{aligned}$$

If, for instance, $i = j = 1$, $\delta(u_i u_j)$ is the total amount of streamwise fluctuating kinetic energy u_1^2 contributed by one isolated eddy per unit thickness of fluid in the z-direction.

Contribution to the mean value of $\overline{u_i u_j}$ from a given hierarchy will be written as $\Delta\overline{u_i u_j}$, and we simply add the energies from each member of the hierarchy since we have a random distribution of these eddies and the mean values of cross-correlations between velocities induced by our given eddy and those of neighbouring eddies will vanish on averaging. This is effectively the assumption used by Townsend. Following the analysis used for obtaining the mean vorticity, we have

$$\Delta\overline{u_i u_j} = \int_z^{\delta} \frac{U_0^2 \delta^2 \phi_{ij}\left(\frac{z}{\delta}, \frac{h}{\delta}\right)}{\lambda_k e \delta} f'_{\mathrm{E}}(h/\delta)\, dh.$$

Following the scaling rules given earlier, i.e. $\lambda_k \sim \delta$ and $e \sim \delta$, we then have

$$\frac{\Delta\overline{u_i u_j}}{U_0^2} \sim \int_{z/\delta}^{1} \phi_{ij}\left(\frac{z}{\delta}, \frac{h}{\delta}\right) f'_{\mathrm{E}}\left(\frac{h}{\delta}\right) d\frac{h}{\delta}$$

or

$$\frac{\Delta u_i u_j}{U_0^2} = I_{ij}\left(\frac{z}{\delta}\right).$$

It should be noted that it is being assumed that there is no contribution to $\delta(u_i u_j)$ from an eddy once z exceeds h. Our computations, assuming that a hierarchy could be replaced by a 'representative' Λ-vortex, show that there is a rapid fall-off once z exceeds δ. Nevertheless, this assumption is not strictly necessary since we can simply redefine δ such that for $z/\delta = O(1)$ this contribution is small.

Here $I_{ij}(z/\delta)$ is equivalent to Townsend's eddy function. He assumed that all eddies were geometrically similar, and did not include the strain number. This has now been 'integrated out', and $I_{ij}(z/\delta)$ represents an eddy hierarchy function.

The value of $\overline{u_i u_j}$ is found simply by summing up the contributions from the various hierarchies thus:

$$\frac{\overline{u_i u_j}}{U_0^2} = \sum_{n=1}^{N} I_{ij}\left(\frac{z}{\delta_1 2^{n-1}}\right) = \sum_{n=1}^{N} I_{ij}\left(\frac{z}{\delta_n}\right), \tag{6.2}$$

assuming a geometrical progression of hierarchies with the scales doubling from one hierarchy to the next. We could go from the discrete system to the distributed system by using the relation given by (5.9), i.e.

$$\frac{\overline{u_i u_j}}{U_0^2} = \sum_{n=1}^{N} I_{ij}\left(\frac{z}{\delta_1 2^{n-1}}\right) \nrightarrow \int_{\delta_1}^{\Delta_E} I_{ij}\left(\frac{z}{\delta}\right)\frac{M}{\delta}\,d\delta. \tag{6.3}$$

We must now consider the properties of the hierarchy function $I_{ij}(z/\delta)$. Here we will invoke the Townsend (1976) boundary conditions. For z/δ small,

$$f_3 \sim \frac{z}{\delta}\psi\left(\frac{x}{\delta}, \frac{y}{\delta}, \frac{h}{\delta}\right),$$

since $f_3(0) = 0$ and we are assuming that we can Taylor-series expand about $z = 0$. The functions f_1 and f_2 are not restricted in this way, and $f_1(0)$ and $f_2(0)$ could be finite, assuming that we are neglecting viscous effects and are allowing slip at the boundary.

$$I_{13} \sim z^*, \quad I_{33} \sim z^{*2}, \quad \text{and} \quad I_{11}, I_{22} \to \text{non-zero values} \quad \text{as} \quad z^* \to 0. \tag{6.4}$$

Here $z^* = z/\delta$. Using (6.3) it can be shown that

$$\frac{\overline{u_i u_j}}{U_0^2} = \int_{z/\Delta_E}^{z/\delta_1} I_{ij}(z^*)\, M \frac{dz^*}{z^*}, \tag{6.5}$$

which is the Townsend result. Conjectured functional forms for $I_{ij}(z^*)$ are shown in Townsend (1976, figure 5.7). From (6.4) and (6.5) it can be shown that†

$$\overline{u_1 u_3}/U_0^2 = K_{13}, \tag{6.6}$$

where K_{13} is a universal constant. Since U_0 has been taken to be constant it follows that we have constant Reynolds shear stress. Hence all the scaling rules developed in §5 for eddy hierarchies are consistent. Furthermore, U_0 can be taken to be U_τ, the friction velocity. Other results that follow are

$$\frac{\overline{u_1^2}}{U_\tau^2} = B_{u_1} - A_{u_1} \ln \frac{z}{\Delta_E}, \tag{6.7}$$

$$\frac{\overline{u_2^2}}{U_\tau^2} = B_{u_2} - A_{u_2} \ln \frac{z}{\Delta_E}, \tag{6.8}$$

$$\frac{\overline{u_3^2}}{U_\tau^2} = B_{u_3}, \tag{6.9}$$

† Townsend's analysis for this is brief, and some details are given in appendix B.

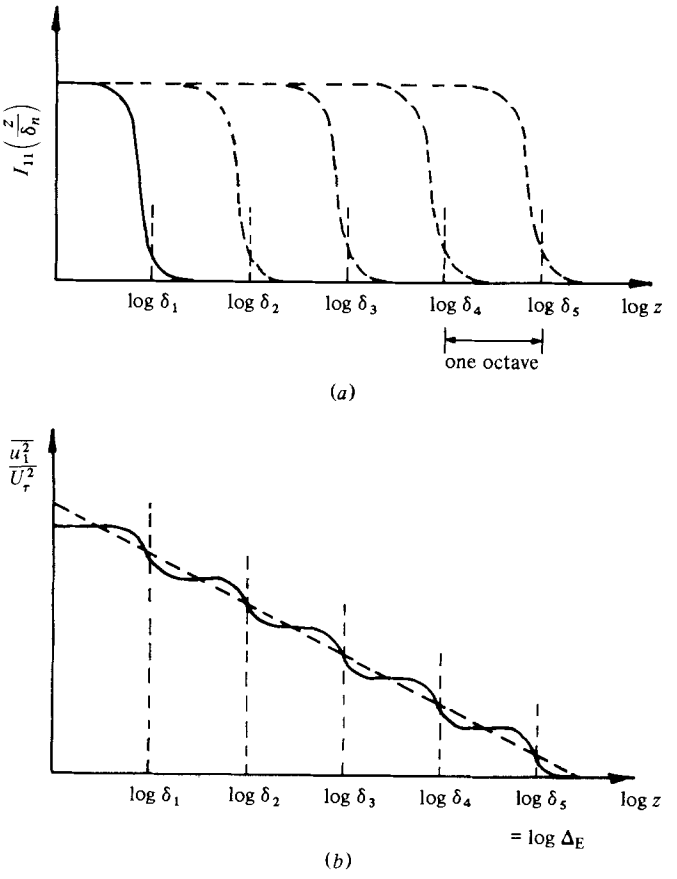

FIGURE 21. Summation of eddy hierarchy functions for $\overline{u_1^2}/U_\tau^2$. (*a*) Functions for various hierarchies. (*b*) Summation of functions.

where A_{u_1}, A_{u_2}, B_{u_1}, B_{u_2} and B_{u_3} are universal constants. These equations were quoted in 'differential form' as laws 3, 4 and 5 in table 1.

A very illustrative way of showing the validity of these relations is to consider the discrete system with the scales of hierarchies doubling:

$$\frac{\overline{u_i u_j}}{U_\tau^2} \sim \sum_{n=1}^{N} I_{ij}\left(\frac{z}{\delta_1 2^{n-1}}\right) = \sum_{n=1}^{N} I_{ij}\left(\frac{z}{\delta_n}\right).$$

$I_{11}(z/\delta_n)$ when plotted semilogarithmically is stretched out at low values of z/δ_n and is approximately constant, and, for z/δ_n of order 1 and higher, the function will be compressed and will drop off very rapidly (see figure 21). Here, these functions for different values of n simply shift bodily horizontally without distortion on the semilogarithmic plot and are each displaced from each other by one octave.

We now sum these functions to give a 'staircase' function shown in figure 21 (*b*). One can see that this staircase function will approximate to the functional form given by (6.7).

Consider now the quantity

$$\frac{\overline{u_1 u_3}}{U_\tau^2} \sim \sum_{n=1}^{N} I_{13}\left(\frac{z}{\delta_1 2^{n-1}}\right) = \sum_{n=1}^{N} I_{13}\left(\frac{z}{\delta_n}\right).$$

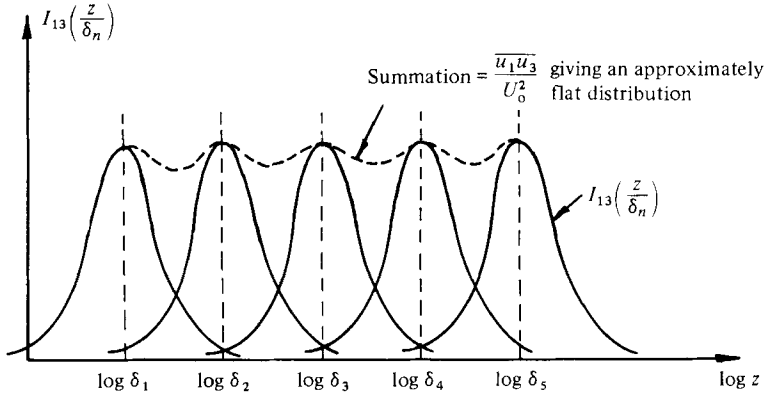

FIGURE 22. Summation of eddy hierarchy functions for Reynolds shear stress.

This is shown in figure 22. Since there are no hierarchies less than δ_1, then $\overline{u_1 u_3}/U_\tau^2$ will drop to zero very rapidly and this would correspond to a region where the Reynolds shear stress is changing rapidly to viscous stresses. The behaviour of $\overline{u_3^2}/U_\tau^2$ will be similar. These 'bumpy' functions and 'staircase' functions will be smoothed out by 'jitter' and randomness or by a genuinely distributed system of hierarchies.

7. The spectrum of turbulence

Fourier transforms and the power-spectral density of signals produced by turbulence are very difficult to interpret or understand. Nevertheless, they are easy to measure and give an indication of how the energy is distributed among the scales. This work was motivated by the idea that modelling of wall turbulence should be consistent with measured spectra and should be linked to the broad-band and mean-flow results.

Unlike models of the past, this model implies that wall turbulence has a granular structure with a characteristic direction. Since local isotropy is no longer operative, a new explanation or argument must be devised for the existence of the $-\frac{5}{3}$ law.

At high frequencies or wavenumbers the power spectrum is influenced mainly by the shape of the eddy signatures, while at lower wavenumbers or frequencies the spectrum is influenced more by how the energy is distributed among the scales. The detailed shape of the signatures become unimportant at these lower wavenumbers. One very useful rule (Bracewell 1978) for the high-frequency end of the spectrum is that, if n is the number of times one has to differentiate a signal to convert it to a delta function, then the smoothed power-spectral density $P(k)$ will asymptote to a law $P(k) \sim k^{-2n}$. Here k is wavenumber or frequency. It has been felt by many workers (see e.g. Townsend 1976) that the finest-scale motions of turbulence are generated by vortex sheets passing the hot-wire probe, and these dissipate the energy of turbulence. From the flow-visualization work of Head & Bandyopadhyay (1981) and Perry *et al.* (1981) these vortex sheets are wound up into rods. The rods could be thought to consist of a 'scroll' of vortex sheet. As such rods are cut through by a sensing probe, the high-pass-filtered signal will be of a sawtooth form provided the vortex sheets are very thin and sharp. Using the Bracewell rule, this should give $P(k) \sim 1/k^2$. This scroll could be something like a Kaden spiral (see e.g. Pullin & Phillips 1981), and

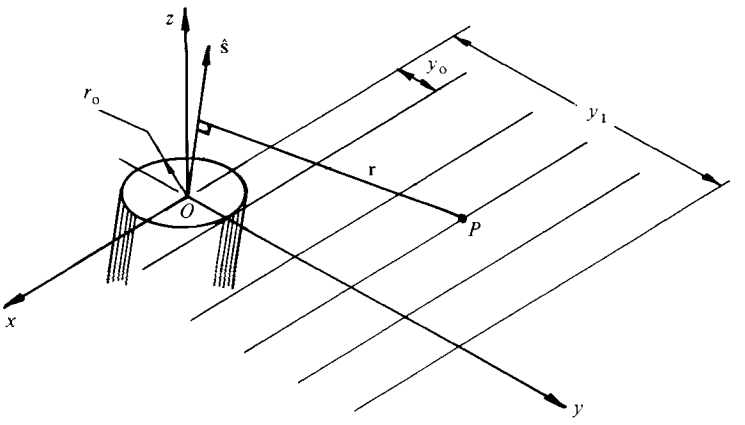

FIGURE 23. Definition of co-ordinates and vectors for velocity-signature analysis.

one would intuitively feel that, since the signature of this is one scale removed from the scale of the sheet itself, then this should be responsible for the $-\frac{5}{3}$ law. With viscous diffusion the sheet will not be perfectly sharp, and, at very high wavenumber, the waveform would appear to have the properties of a triangular wave. Using the Bracewell rule, this leads to $P(k) \sim 1/k^4$. It can be seen that the $-\frac{5}{3}$ law simply does not fit into this scheme. Out of curiosity, we devised a waveform with a $-\frac{5}{3}$ law spectrum to see what it might look like. Using the Bracewell rule, together with the concept of 'fractional differentiation', a wave with a $\frac{1}{6}$ power-law cusp would give the required result. This needs to be differentiated '$\frac{5}{6}$ times' to give $n = \frac{5}{6}$, and hence the $-\frac{5}{3}$ law. This was also checked numerically using a fast-Fourier-transform computer program. It seems unlikely that the $-\frac{5}{3}$ law comes from such eddy signatures. Rather, if it exists, it seems more likely to be related to the distribution of scales of signatures.

We found that a far more fruitful approach to this question was to ignore the details of the rod altogether, or at least assume that the vorticity is smeared out according to the similarity relation given by (2.4). It is found that all of the salient properties of the spectrum can be generated from the signatures and distribution of the signatures existing in the irrotational fluid surrounding the vortex rods. This will now be demonstrated.

In order to keep the description simple and analytical, some simplifications will be made. Let it be assumed that the spectral contribution from each hierarchy can be derived from one representative eddy. Figure 23 shows one 'leg' of the eddy being sectioned by a plane of constant z. If we imagine that we have a hot-wire probe held stationary and that the eddy is being convected past in the x-direction, then the signature as seen by the probe can be calculated by determining $\mathbf{U}$ along the lines of constant y in the (x, y)-plane. To avoid the complications involved with convection velocities, imagine that the vector field is temporarily 'frozen', and the signatures will be Fourier decomposed in terms of the x-component wavenumber k.

By applying the Biot–Savart law in conjunction with (2.4), it can be shown that

$$\mathbf{U} = \Omega_1 r_0^2 \{\hat{\mathbf{s}} \times \mathbf{r}\} \{1 - \exp(-\tfrac{1}{2}|\mathbf{r}|^2/r_0^2)\}/|\mathbf{r}|^2, \tag{7.1}$$

or, assuming solid-body rotation within the rod,

$$\left.\begin{aligned} \mathbf{U} &= \frac{K}{2\pi}\frac{\{\hat{\mathbf{s}}\times\mathbf{r}\}}{|\mathbf{r}|^2} \quad (|\mathbf{r}| > r_0), \\ \mathbf{U} &= \frac{K}{2\pi}\frac{\{\hat{\mathbf{s}}\times\mathbf{r}\}}{r_0^2} \quad (|\mathbf{r}| < r_0), \end{aligned}\right\} \tag{7.2}$$

where K is the circulation of the vortex rod and r_0 in (7.2) is the rod radius. All other symbols are defined in figure 23.

We will imagine that we are making a series of 'cuts' of uniform probability between O and y_1. The magnitude of the signatures reaches a maximum at $y_0 (= r_0)$, and for $0 < y < y_0$ it drops rapidly to zero for the U_1 component. The distance y_1 represents the maximum distance from the rod we can go before experiencing the influence of the other leg or the legs of other vortices. The analysis is therefore using the signatures of one isolated rod. Of course, in future studies, the full Λ-vortex and arrays of such vortices should be used in a computer simulation.

Equation (7.2) gives the following velocity signature for U_1:

$$U_1 = -\frac{Q}{y}\frac{1}{X_*^2+\hbar^2}. \tag{7.3}$$

Here $Q = KA_1\hbar^2/2\pi g$, where A_1, $\hbar$ and g are constants that depend on the direction cosines of the vector $\hat{\mathbf{s}}$. This is expressed in its simplest form by an appropriate choice of the origin for x. Also $X_* = (x-a)/y$, where a is the shift in the origin for x, and a/y depends on the direction cosines. It can be shown that the amplitude of the signature $\sim 1/y$. The U_1 signature is an even 'bell-shaped' function, and the other components are a combination of an even and an odd function.

The Fourier transform of the U_1 velocity signature defined by

$$X_1(k) = \frac{1}{2\pi}\int_{-\infty}^{\infty} U_1(x)\, e^{-ikx}\, dx \tag{7.4}$$

turns out to be† $$X_1(k_1) = -\frac{Q}{2\hbar}\, e^{-k_1 y}, \tag{7.5}$$

where $k_1 = k\hbar$; $\hbar$ is a constant of order unity and depends on direction cosines of the vector $\hat{\mathbf{s}}$. It can be shown that the functional form given by (7.5) is applicable for all three components of velocity.

Consider only the U_1 signature given by (7.5). This is the Fourier transform of a transient pulse. Imagine a train of such pulses arranged randomly in the x-direction with a mean spacing S and that the vorticity sign (or the effective sign of y) can be positive or negative with equal probability. It can be shown that the power-spectral density is given by

$$P(k_1, y) = 2\pi|X_1(k_1, y)|^2/S. \tag{7.6}$$

This equation will be true provided cross-products between neighbouring pulses make no contribution to the spacially averaged two-point correlation coefficient for points separated along the x-direction. An example where this is not true is for periodic

† An interesting historical point can be found from Hinze (1959). In previous work, the auto-correlation functions were often assumed to be exponential, and these gave spectra having functional forms given by (7.3). We have reversed the usual assumptions. Here, signals and autocorrelations of U_1 are bell-shaped and the spectra exponential.

pulses. This would give a periodic correlation coefficient and a power-spectral density consisting of Dirac delta functions. The 'smoothed' power-spectral density would then need to be used in the following discussions. It will be assumed that the contribution to the spectral energy by 'cuts' $y < y_0$ are negligible.

Imagine that we have a collection of signature trains all at different y. Given that the probabilities of all 'cuts' in the interval $0 < y < y_1$ are equally likely, it can be shown that the ensemble-averaged or smoothed power-spectral density is then given by

$$F(k_1) = \frac{1}{y_1}\int_{y_0}^{y_1} P(k_1, y)\, dy. \tag{7.7}$$

From (7.6) and (7.7)

$$F(k_1) = \frac{1}{y_1}\frac{\pi^2 Q^2}{2S}\frac{1}{k_1 \hbar^3}\{\exp(-2k_1 y_0) - \exp(-2k_1 y_0(y_1/y_0))\}. \tag{7.8}$$

Since all hierarchies are geometrically similar, all length scales will scale with y_0, and Q will scale such that $Q \sim U_\tau y_0$, where U_τ is the characteristic velocity scale of all the hierarchies (and is also the friction velocity).

Let (7.8) represent the smallest observed hierarchy, which will be labelled $n = 1$. If the total number of observed hierarchies is N_0, the resulting power-spectral density Φ will be given by

$$\frac{\Phi(k_1 y_0)}{U_\tau^2} \sim \sum_{n=1}^{N_0} \frac{1}{k_1 y_0}\{\exp(-2k_1 y_0 2^{(n-1)}) - \exp(-2k_1 y_0 (y_1/y_0)\, 2^{(n-1)})\}. \tag{7.9}$$

Here Φ is the energy per unit non-dimensional wavenumber $k_1 y_0$. The scale y_0 for the nth hierarchy is $y_0 2^{n-1}$.

From figure 14 it can be seen that as we go away from the wall the total number of observed hierarchies diminishes, i.e. N_0 decreases. Also, y_0 is the smallest length scale of the smallest observed hierarchy and this will decrease as we approach the wall; the smallest value will then be proportional to the Kline scaling on a smooth surface. The ratio y_1/y_0 will be universal and is associated with the geometry of the representative eddy of a given hierarchy. A continuous distribution of scales would give much the same result but an exponential integral is involved.

Figure 24 shows (7.9) for different hierarchies with $y_1/y_0 = 10$, i.e. it is assumed that the ratio of rod diameter to leg spacing is of this order. It can be seen that as the wavenumber is decreased the spectrum goes from an exponential to a -1 power law, with a short section that could be interpreted as a $-\frac{5}{3}$ law. However, we feel that this is not of significance, and that the law where the various hierarchies 'peel off' is the -1 power law. The scale y_1 of the largest hierarchy determines the low-wavenumber 'cut-off' or 'levelling out' and the scale y_0 of the smallest hierarchy determines the high-wavenumber cut-off. The spectral results of Perry & Abell (1977) taken in the wall region of a pipe are shown in figure 25. The existence of a -1 power law is obvious. This law was deduced by Perry & Abell using a 'region of overlap' argument based on dimensional analysis. The departure from the -1 power law occurs at approximately $k_1 z = 1$ in the experiments and at $k_1 y_0 \simeq 10^{-1}$ according to (7.9). This implies that, at level z, the smallest 'representative eddy' of significance has $y_1 \simeq O(z)$. This is of the right order.

It is very instructive to look at spectra far from the wall. Here the number N_0 of observed hierarchies fall off considerably and the spectra should follow the pattern

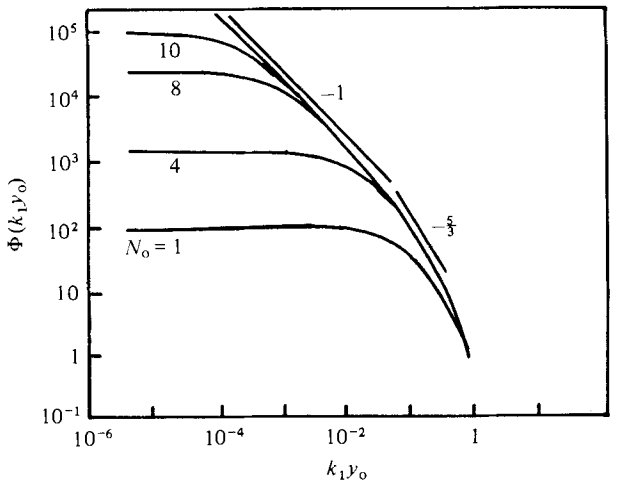

FIGURE 24. Equation (7.9) for various numbers of observed hierarchies: $\log \Phi(k_1y_0)$ versus $\log k_1y_0$; $y_1/y_0 = 10$.

given in figure 24. Figure 26 (*a*) shows some results of Abell & Perry (1974) for a smooth pipe. Again, the similarity with the computed results given in figure 24 is very encouraging. As a matter of interest, figure 26 (*b*) shows some rough-walled-pipe results taken outside the wall similarity region. The results show a similar behaviour. We would expect the smallest hierarchy scale δ_1 at the wall to scale with ϵ, the roughness scale. Unfortunately, no measurements exist for the wall similarity region for this case.

The model is of course simplified. Spectral information concerned with the vortex shape and the plane-strain processes is missing. However, the authors contend that the inclusion of this information will not alter the general behaviour, and will simply be hidden or 'buried' in the -1 power-law region, or else be removed by smoothing.

The scaling of Perry & Abell results given in figure 25 suggest that for the wall region but beyond the buffer zone

$$\Phi(k_1z)/U_\tau^2 = f(k_1z), \tag{7.10}$$

where Φ is now the energy per unit non-dimensional wavenumber k_1z, and this appears valid right up to high wavenumbers. This is reasonable, since at a given z the smallest eddy of significance observed will scale approximately with z since, if it is smaller, it will not be seen and, if it is larger, it will not be the smallest eddy.

In the energy-containing region

$$\frac{\Phi(k_1z)}{U_\tau^2} = \frac{A}{k_1z}, \tag{7.11}$$

where A is a universal constant. Figure 27 shows the spectra with appropriate 'cut-offs'. B and $\mathscr{M}$ are universal constants. The broad-band quantity $\overline{u_1^2}/U_\tau^2$ is obtained approximately from the integral

$$\frac{\overline{u_1^2}}{U_\tau^2} = \int_0^\infty \frac{\Phi(k_1z)}{U_\tau^2} = \int_0^{Bz/\Delta_E} \frac{A\Delta_E}{B}\, d(k_1z) + \int_{Bz/\Delta_E}^{\mathscr{M}} \frac{A}{k_1}\, d(k_1z),$$

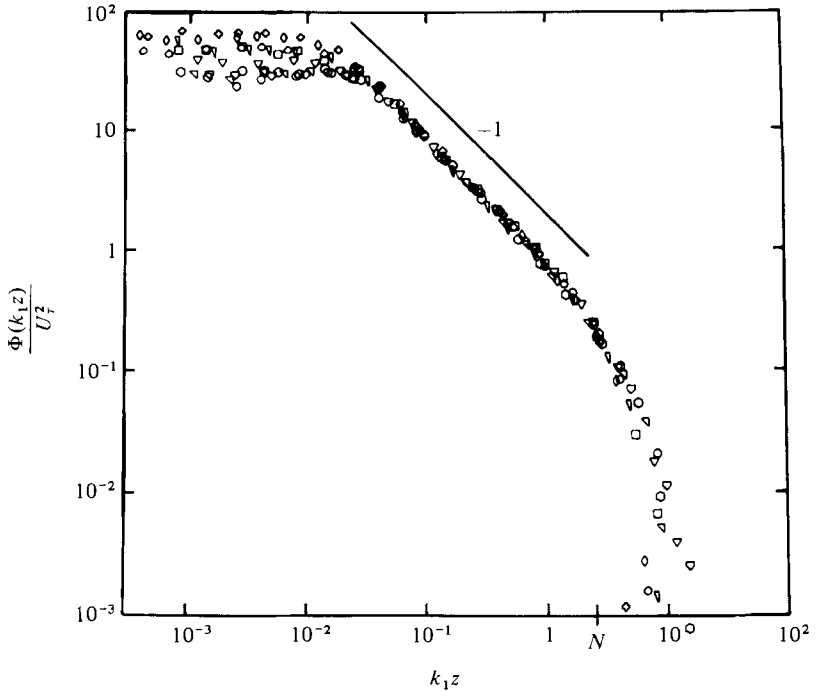

FIGURE 25. Smooth-wall longitudinal spectra for the wall similarity range $z_+ > 100$ and $z/R < 0{\cdot}1$. Reynolds-number range $Re = 80 \times 10^3$–260×10^3. R is pipe radius, and here

$$\int_0^\infty \Phi(k_1 z)\, d(k_1 z) = \overline{u_1^2}.$$

	$Re \times 10^{-3}$	y^+	y/R	$\overline{U}/u_\tau$
○	80	150	0·0934	17·6
□	120	100	0·043	16·6
▽	120	150	0·0645	17·59
⬡	120	200	0·086	18·3
◇	180	104	0·03	16·6
◁	180	138	0·04	17·31
⬡	180	275	0·08	19·2
✣	260	148	0·03	17·6
◇	260	246	0·05	18·8
◁	260	444	0·09	20·4

which could be written in the form

$$\frac{\overline{u_1^2}}{U_\tau^2} = B_{u_1} - A_{u_1} \ln \frac{z}{\Delta_E},$$

which is the Townsend result given earlier ((6.7)).

The results of Abell & Perry (1974) and Perry & Abell (1975, 1977) were obtained by a stationary probe and frequencies had to be converted to wavenumbers k_1 by the use of an assumed convection velocity. The small eddies at the wall will be convecting themselves 'back' relative to a field induced by the larger eddies. The largest eddies, on the other hand, will be convecting themselves back relative to the free stream. Since the characteristic velocity of each hierarchy is the same, then, relative

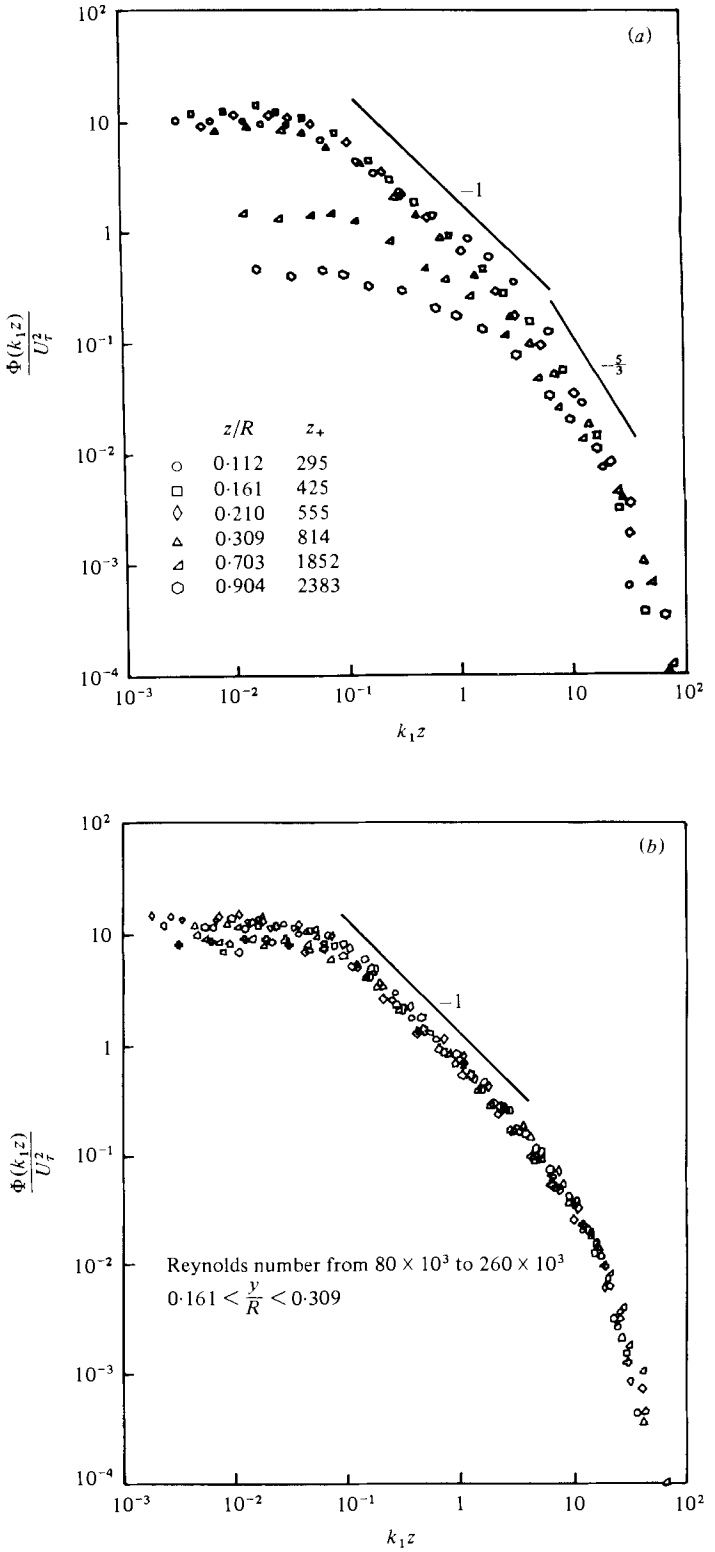

FIGURE 26. For caption see opposite.

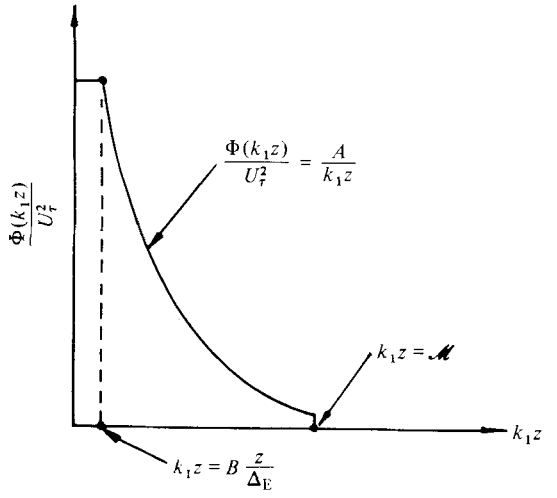

FIGURE 27. Linear plot of spectrum.

to a stationary observer, the largest eddies will have the highest convection velocity (and this will be in the direction of the free stream). Perry & Abell (1975, 1977) discussed this spread in phase velocities and assumed that the highest wavenumbers would be convected approximately at the local mean velocity at a given level z. This is probably not correct, particularly for the lower wavenumbers at a fixed level z. However, the above authors found that an incorrectly inferred wavenumber in the -1 region of the spectrum made no difference. It simply shifted the data points along the -1 line. Thus the assumption that all wavenumbers are convected at the local mean velocity at a given level z will not alter the general features of the spectrum. This assumption was used in the spectral data presented.

Although Perry & Abell (1977) also incorporated the $-\frac{5}{3}$ power law in their scaling scheme by a further 'region-of-overlap' argument, it would appear that this law is a 'red herring', at least in wall turbulence. However, the existence of the law is very obvious in other types of turbulence. If we return to (7.6) and redistribute the energy among the hierarchies such that

$$\frac{\Phi(k_1 y_0)}{U_\tau^2} \sim \sum_{n=1}^{N_0} \frac{2^{\frac{2}{3}(n-1)}}{k_1 y_0} \left\{ \exp\left[-2k_1 y_0 2^{n-1}\right] - \exp\left[-2k_1 y_0 \left(\frac{y_1}{y_0}\right) 2^{n-1}\right] \right\}, \tag{7.12}$$

then one obtains a family of spectra for different N_0, as shown in figure 28. All low-wavenumber 'peel-offs' occur from a $-\frac{5}{3}$ line. Figure 29(*a*) shows a turbulent jet. The eddy structure in this jet is quite granular, with a characteristic direction, but the resulting spectra given in figure 29(*b*) shows an extensive $-\frac{5}{3}$ law without any evidence of a -1 law. Thus it would appear that there are different sorts of turbulence, and the $-\frac{5}{3}$ law results from a different distribution of energy from that found in wall turbulence. The physical reason for this is not yet understood, and this idea needs to be pursued.

FIGURE 26. Measured spectrum function $\Phi(k_1 z)/U_\tau^2$ in a pipe for regions beyond the wall similarity zone. (*a*) Smooth pipe. (*b*) Rough pipe. Here $\int_0^\infty \Phi(k_1 z)\, d(k_1 z) = \overline{u_1^2}$.

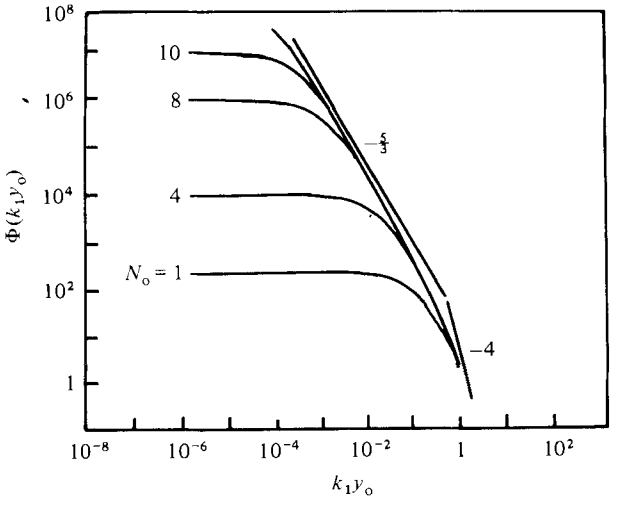

FIGURE 28. Equation (7.12) for different numbers of observed hierarchies.†

8. Conclusions and discussions

Turbulent boundary layers can be thought of as a forest of Λ-type vortices which originates from the wall. Computer calculations show that these vortices have the correct transport properties. Fluid is lifted from the wall and replaced by fluid from above. The hypothesis of vorticity cancellation enables one to regard the vortices as being surrounded by irrotational fluid. It is this vorticity cancellation that makes the problem tractable. In the transport of heat there is no analogous thermal cancellation, and so the problem is intractable at this stage without numerical simulations.

The Λ-shaped vortices commence their growth from the wall, and are initially at the Kline scaling. During their process of roll-up, viscous sublayer material is rolled up in a sheet, and this sheet rolls up to form rods. Once the roll-up process ceases, the circulation in the rod remains constant, and the Λ-vortex stretches under its own mutual induction with its image to give, in the large, plane strain, at least for the vortices assumed here. The rods appear locally to undergo axisymmetrical strain. All these motions have been observed in trip-wire vortices, and are predicted by the Biot–Savart law. The plane strain brings the legs of the vortex together, and vorticity cancellation takes place by viscous diffusion, leading to the death of the eddy. A hierarchy of scales of these eddies must exist to obtain a logarithmic mean-velocity profile with constant Reynolds shear stress for arbitrary large z_+ for $\Delta_E U_\tau/\nu \to \infty$. These hierarchies must be geometrically similar and the circulation in the vortex rods must scale with the hierarchy scale δ. This geometrical similarity includes all length scales associated with the eddy, including its mean streamwise and spanwise spacing. Hence all hierarchies have the same characteristic velocity scale. Two possible models for the existence of the various scales of hierarchies are described. One is the vortex-pairing process, and this leads to a discrete system of hierarchies where the scales go in a geometrical progression with a factor of 2. This model requires plane strain to

† Equation (7.12) has recently been computed for 20 hierarchies and the results asymptote even closer to the $-\frac{5}{3}$ law.

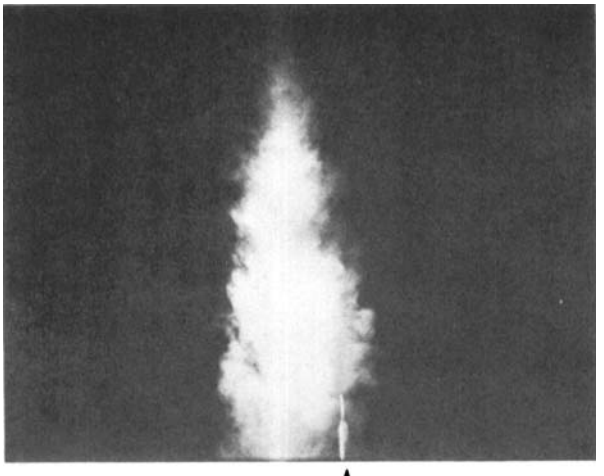

(*a*)

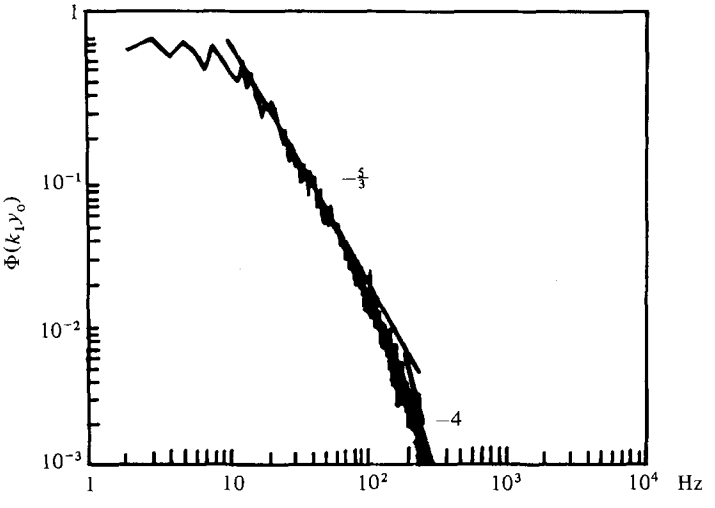

(*b*)

FIGURE 29. Turbulent jet. (*a*) Flow pattern. (*b*) Measured spectrum; ensemble average of 40 runs. Reynolds number based on tube outlet diameter = 3000.†

explain the continuous distribution of the logarithmic profile. However, jitter would tend to smear out the scale distributions to give an inverse-power p.d.f.; plane strain is then not necessary to explain the logarithmic distribution.

If we have a continuous distribution of hierarchy scales, then it can be shown that any hierarchy function $f(z, \delta)$ will lead to a logarithmic profile, i.e.

$$\frac{d\overline{U}_1}{dz} = \int_{\delta_1}^{\Delta_E} f(z, \delta)\, p_H(\delta)\, d\delta,$$

† By moving the probe further downstream in a jet we have recently found that the extent of the $-\frac{5}{3}$ law increases.

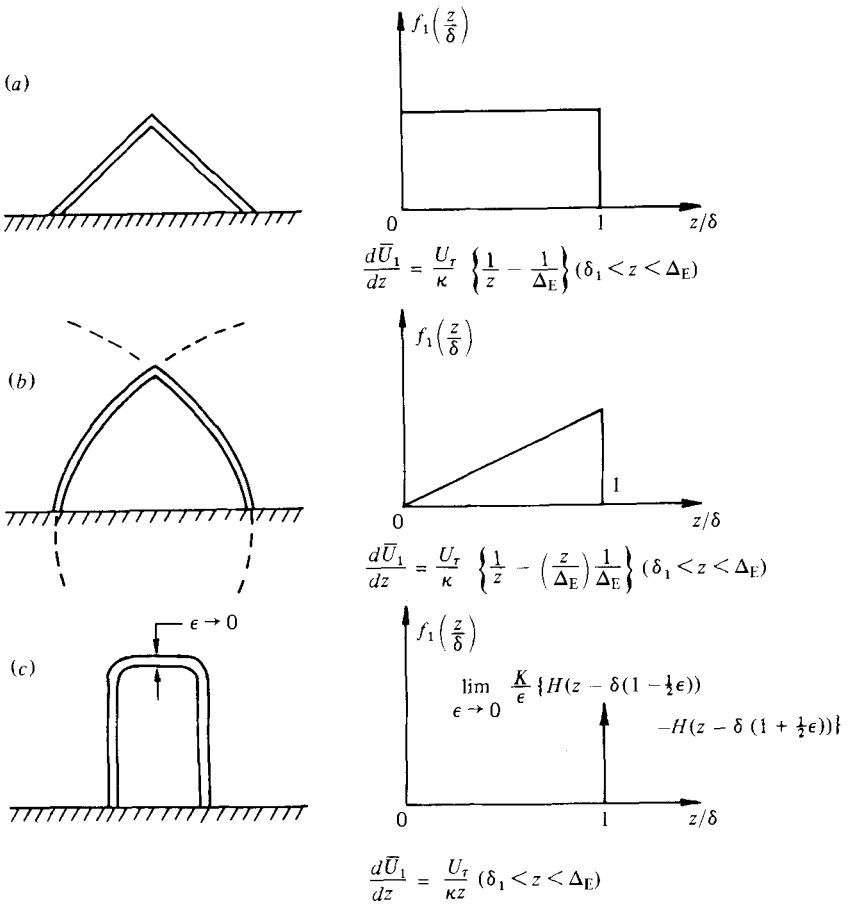

FIGURE 30. Various eddy shapes and resulting distributions of $d\bar{U}_1/dz$ without plane strain or stretching. (*a*) True Λ-vortex; (*b*) parabolic 'Λ' vortex; (*c*) rectangular 'Λ' vortex.

provided $f(z,\delta) = (U_\tau/\delta)f_1(z/\delta)$ and $p_H(\delta) = M/\delta$. $d\bar{U}_1/dz = U_\tau/\kappa z$ will occur over some range for $\delta_1 < z < \Delta_E$ no matter what form f_1 takes, provided it does not have a singularity at $z/\delta \to 0$. Figure 30 shows various eddy shapes and the laws given without plane strain or stretching. The effect of stretching is simply to 'smear' out $f_1(z/\delta)$ and hence reduce the range of validity of the logarithmic profile. The laws given in table 1 for the velocity are simply not sufficient to pin down precisely the eddy shape and its motion. If some further information could be obtained from the temperature distribution, this would help to narrow down the possibilities. The other alternative is to establish more laws based on higher moments of probability (see e.g. Frenkiel & Klebanoff 1973).

So far we have dealt mainly with the wall region. There is no reason why our model should not be applicable with some detailed modifications to the outer flow. However, at the moment, the model predicts a deviation below the logarithmic law as $z/\Delta_E \to 1$. This would give a negative Coles wake factor (see Coles 1956). A gradual departure from geometrical similarity as $\delta/\Delta_E \to 1$ and a modification of $p_H(\delta)$ would probably cure this anomaly.

For a long time, the concept of vortex pairing was resisted by the authors. The

idea of two Λ-vortices pairing to produce one Λ-vortex with its circulation doubled and to have an increase in scale so as to belong to a higher hierarchy appears to be inconsistent with the conservation of kinetic energy. However, this is true only if we are considering two isolated Λ-vortices producing one isolated Λ-vortex. In reality, the Λ-vortices are not isolated but are arranged in an array. The contribution of kinetic energies from the Λ-vortices must be broken up into a mean-flow contribution and a fluctuating contribution. The pairing process may cause an increase in turbulent kinetic energy at the expense of the mean-flow kinetic energy. There is no simple way of deciding, on the basis of energy considerations, whether this pairing process is possible once interactions with neighbouring vortices and mean-flow fields are taken into account. Pairing has been observed in other flow situations, such as in free shear layers, jets and wakes both experimentally and computationally (see e.g. Winant & Browand 1974; Brown & Roshko 1974; Acton 1980). However, we have yet to observe this pairing in boundary layers. The more easily observed trip-wire vortices have been studied for some time, and we have so far failed to 'coax' them to pair.

The continuously growing eddy model is an attractive possibility. Here the eddy continues to draw vorticity from the wall, and its circulation is assumed to increase in proportion with its scale δ, its shape being preserved during this process. Once the process is interrrupted, plane strain commences, leading to the ultimate death of the eddy. The likelihood of survival during the growth must diminish with scale δ, leading to the appropriate distribution of hierarchy scales. This model gives a genuinely continuous distribution of hierarchy scales. However, it should be pointed out that there is no obvious mechanism based on the Biot–Savart law for this continuous roll-up with a 'self-preserving-shape' eddy, nor has its existence been definitely established.

Turbulence spectra that have all the correct properties can be derived by the use of eddy signatures derived from potential-flow vortices which have characteristic directions. The distribution of energy among the scales follows directly from the scaling laws needed to give the logarithmic profile and constant Reynolds shear stress. The use of local isotropy and energy cascades does not appear to be relevant. The use of the potential-flow Λ-vortex in obtaining a link between the mean flow, Reynolds shear stress, turbulence intensities and spectra in wall turbulence looks promising.

The authors wish to acknowledge the financial assistance of the Australian Research Grants Committee, The National Energy Research, Development and Demonstration Council and the Australian Institute of Nuclear Science and Engineering.

Appendix A

Equation (5.6) can be written as a particular case of

$$\frac{d\overline{U}_1}{dz} = \sum_{n=1}^{N} f(z, (1-\epsilon)^{-(n-1)}\delta_1), \tag{A 1}$$

with $\epsilon = \frac{1}{2}$. Now (A 1) can be written as

$$\sum_{n=1}^{N} f(z, (1-\epsilon)^{-(n-1)}\delta_1) = \int_{\delta_1}^{\Delta_E} f(z,\delta) \sum_{n=-\infty}^{\infty} \mathscr{D}(\delta - (1-\epsilon)^{-(n-1)}\delta_1)\, d\delta, \tag{A 2}$$

where $\mathscr{D}$ is the Dirac delta function.

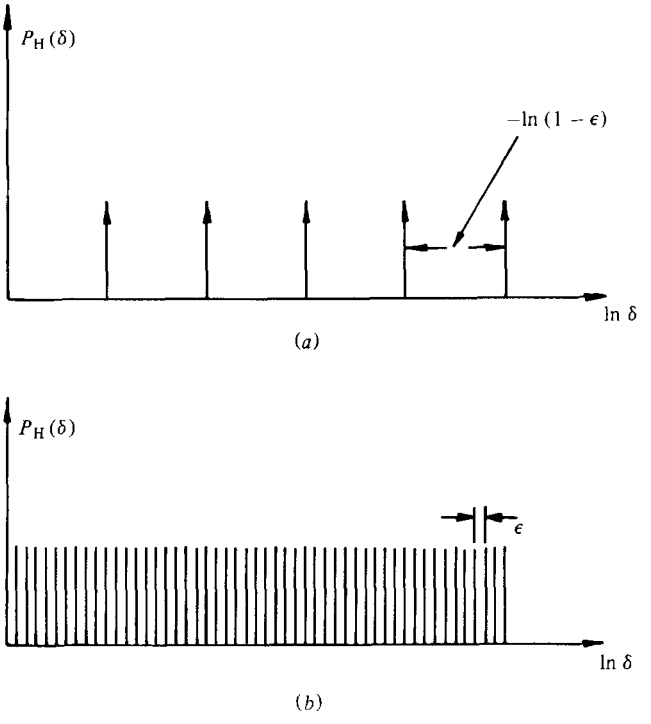

FIGURE 31. Equation (A 1): (*a*) ϵ finite; (*b*) $\epsilon \to 0$.

We would like to write

$$\frac{d\overline{U}_1}{dz} = \int_{\delta_1}^{\Delta_E} f(z,\delta)\, p_H(\delta)\, d\delta, \tag{A 3}$$

where $p_H(\delta)$ is a finite, smooth continuous function which possesses properties similar to our geometrical progression. With the discrete system

$$p_H(\delta) = \sum_{n=-\infty}^{\infty} \mathscr{D}(\delta - (1-\epsilon)^{-(n-1)}\delta_1). \tag{A 4}$$

Equation (A 4) is shown plotted semilogarithmically in figure 31 (*a*). To make $p_H(\delta)$ continuous, we need to take $\epsilon \to 0$ and then 'smooth' the function. Firstly, taking $\epsilon \to 0$ gives the diagram shown in figure 31 (*b*). The spacing between the spikes is given by

$$-\ln(1-\epsilon) \to +\epsilon + \tfrac{1}{2}\epsilon^2 + \tfrac{1}{3}\epsilon^3 + \ldots$$

as $\epsilon \to 0$, and in the limit the spacing is ϵ.

Let $p_{Hs}(\delta)$ be the smooth value of $p_H(\delta)$ defined as

$$p_{Hs}(\delta) = \frac{1}{\Delta\delta}\int_{\delta}^{\delta+\Delta\delta} p_H(\delta)\, d\delta. \tag{A 5}$$

For $\Delta\delta$ sufficiently small, and ϵ even smaller $p_{Hs}(\delta) = dN/d\delta$, where dN is the number of unit-area spikes in the interval $d\delta$. But

$$\frac{dN}{d\ln\delta} = \frac{1}{\epsilon} = \frac{dN}{d\delta}\frac{d\delta}{d\ln\delta}. \tag{A 6}$$

Hence $p_{Hs}(\delta) = 1/\epsilon\delta$.

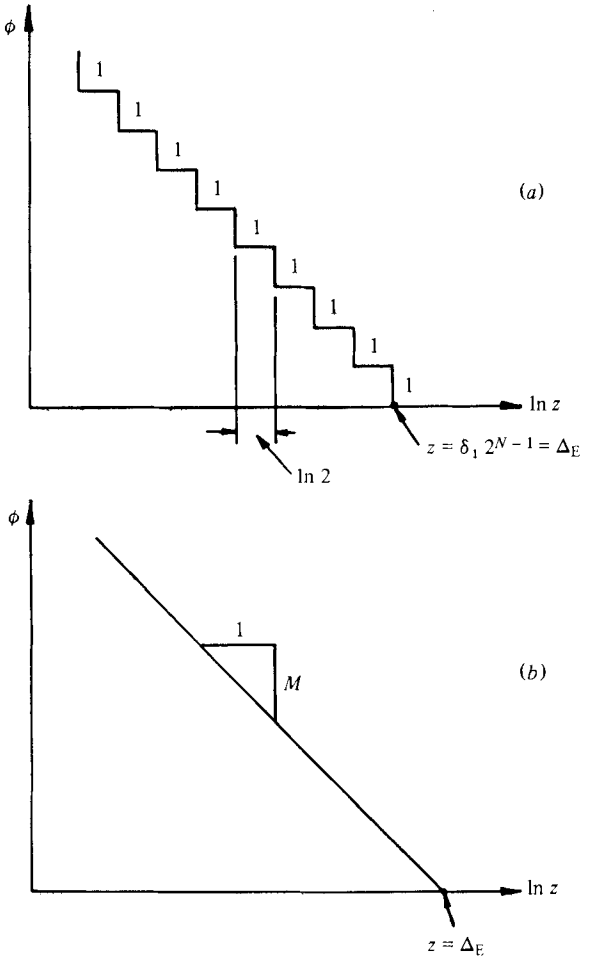

FIGURE 32. Comparison of function ϕ weighted by a discrete and a distributed p.d.f.

Unfortunately, as $\epsilon \to 0$ this does not converge. A more appropriate function for $p_{\mathrm{H}}(\delta)$ is the smoothed value

$$p_{\mathrm{Hs}}(\delta) = M/\delta, \tag{A 7}$$

and is the p.d.f. of a logarithmic probability distribution. Thus we could say

$$\sum_{n=1}^{N} f(z, \delta_1 2^{n-1}) \doteq \int_{\delta_1}^{\Delta_{\mathrm{E}}} f(z, \delta) \frac{M}{\delta} d\delta. \tag{A 8}$$

Consider the following example, which shows a comparison between the distributed and discrete system. Suppose we wished to sum together a series of functions $f(z, \delta)$, where δ is going in geometrical progression with a factor of 2 to give a function ϕ. Suppose

$$f(z, \delta) = \{1 - H(z - \delta)\}.$$

In the discrete system, the resulting function ϕ would be given by

$$\phi = \sum_{n=1}^{N} \{1 - H(z - \delta_1 2^{n-1})\},$$

and this is shown plotted semilogarithmically in figure 32(*a*). For a distributed system

$$\phi = \int_{\delta_1}^{\Delta_E} f(z,\delta)\frac{M}{\delta}d\delta$$

$$= \int_{z}^{\Delta_E} \frac{M}{\delta}d\delta = -M\ln\frac{z}{\Delta_E}.$$

This is shown plotted semilogarithmically in figure 32(*b*).

Appendix B

Consider the integral

$$\frac{\overline{u_1 u_3}}{U_0^2} = \int_{z/\Delta_E}^{z/\delta_1} I_{13}(z^*)\, M\frac{dz^*}{z^*}.$$

For z^* small, let $I_{13}(z^*) = Qz^*$, where Q is a universal constant. Let k be a universal value of z^* such that it is the outer limit of $I_{13}(z^*) = Qz^*$.

We will now integrate in two regions:

$$\frac{\overline{u_1 u_3}}{U_0^2} = \int_{z/\Delta_E}^{k} QM\,dz^* + \int_{k}^{z/\delta_1} I_{13}(z^*)\, M\frac{dz^*}{z^*}.$$

Now for $\delta_1 < z \ll \Delta_E$

$$\frac{\overline{u_1 u_3}}{U_0^2} = QM\left\{k - \frac{z}{\Delta_E}\right\} + \int_{k}^{\infty} I_{13}(z^*)\, M\frac{dz^*}{z^*}.$$

Note that, for $z^* > O(1)$, $I_{13} \to I_{13}(\infty) \to 0$. Therefore

$$\frac{\overline{u_1 u_3}}{U_0^2} \simeq QMk + K_1,$$

where K_1 is a universal constant. Therefore, $\overline{u_1 u_3}/U_0^2 = K_{13}$, where K_{13} is a universal constant. Equations (6.7)–(6.9) are found by a similar technique, noting the various Townsend boundary conditions given by (6.4).

REFERENCES

Abell, C. J. & Perry, A. E. 1974 Smooth and rough wall pipe flow longitudinal turbulence spectral data. *University of Melbourne Dep. of Mech. Engng, Internal Rep.* FM-6.

Acton, E. 1980 Modelling of large eddies in an axisymmetric jet. *J. Fluid Mech.* **98**, 1–36.

Bakewell, H. P. & Lumley, J. L. 1967 Viscous sublayer and adjacent wall region in turbulent pipe flow. *Phys. Fluids* **10**, 1880.

Bandyopadhyay, P. & Head, M. R. 1979 Visual investigation of turbulent boundary layer structure. *Cambridge University Engng Dept Film.*

Blackwelder, R. F. 1978 The bursting process in turbulent boundary layer. In *Proc. Workshop on Coherent Structure of Turbulent Boundary Layers, Lehigh University*, p. 211.

Bracewell, R. N. 1978 *The Fourier Transform and its Application.* McGraw-Hill.

Brown, G. L. & Roshko, A. 1974 On density effects and large structure in turbulent mixing layers. *J. Fluid Mech.* **64**, 775.

Clauser, F. H. 1956 The turbulent boundary layer. *Adv. Appl. Mech.* **4**, 1–51.

Coles, D. 1956 The law of the wake in the turbulent boundary layer. *J. Fluid Mech.* **1**, 191–226.

COLES, D. & HIRST, A. E. 1968 *Proc. AFSOR-IFP Stanford Conf. on Turbulent Boundary Layer Prediction*, vol. 2.

CORRSIN, S. 1957 *Proc. Symp. on Naval Hydrodynamics. NAS-NRC Publ.* no. 515, p. 373.

FRENKIEL, F. N. & KLEBANOFF, P. S. 1973 Probability distributions and correlations in a turbulent boundary layer. *Phys. Fluids* **16**, 725–737.

GRASS, A. J. 1971 Structural features of turbulent flow over smooth and rough boundaries. *J. Fluid Mech.* **50**, 233.

HAMA, F. R. 1954 Boundary layer characteristics for smooth and rough surfaces. *Trans. Soc. Naval Arch. Mar. Engrs* **62**, 333–351.

HEAD, M. R. & BANDYOPADHYAY, P. 1981 New aspects of turbulent boundary-layer structure. *J. Fluid Mech.* **107**, 297–337.

HINZE, J. O. 1959 *Turbulence*. McGraw-Hill.

HOFFMAN, P. H. & PERRY, A. E. 1979 The development of turbulent thermal boundary layers on flat plates. *Int. J. Heat Mass Transfer* **22**, 39–46.

KADAR, B. A. & YAGLOM, A. M. 1972 Heat and mass transfer laws for fully turbulent wall flows. *Int. J. Heat Mass Transfer* **15**, 2329–2353.

KLINE, S. J. 1967 Observed structural features in turbulent and transitional boundary layers. In *Fluid Mechanics of Internal Flow* (ed. G. Sovran). Elsevier.

KLINE, S. J., REYNOLDS, W. C., SCHRAB, F. A. & RUNSTADLER, P. W. 1967 The structure of turbulent boundary layers. *J. Fluid Mech.* **30**, 741–773.

MILLIKAN, C. D. 1938 A critical discussion of turbulent flows in channels and circular tubes. In *Proc. 5th Congress Appl. Mech.*, p. 386–392.

PERRY, A. E. & ABELL, C. J. 1975 Scaling laws for pipe-flow turbulence. *J. Fluid Mech.* **67**, 257–271.

PERRY, A. E. & ABELL, C. J. 1977 Asymptotic similarity of turbulence structures in smooth- and rough-wall pipes. *J. Fluid Mech.* **79**, 785–799.

PERRY, A. E., BELL, J. B. & JOUBERT, P. N. 1966 Velocity and temperature profiles in adverse pressure gradient turbulent boundary layers. *J. Fluid Mech.* **25**, 299–320.

PERRY, A. E. & FAIRLIE, B. D. 1974 Critical points in flow patterns. *Adv. Geophys.* B **18**, 299–315.

PERRY, A. E., LIM, T. T. & CHONG, M. S. 1980 The instantaneous velocity field of coherent structures in coflowing jets and wakes. *J. Fluid Mech.* **101**, 243–256.

PERRY, A. E., LIM, T. T. & TEH, E. W. 1981 A visual study of turbulent spots. *J. Fluid Mech.* **104**, 285–403.

PULLIN, D. I. & PHILLIPS, W. R. C. 1981 On the generalization of Kaden's problem. *J. Fluid Mech.* **104**, 45–53.

REYNOLDS, W. C., KAYS, W. M. & KLINE, S. J. 1958 *NASA Memo.* no. 12–1–58W.

THEODORSEN, T. 1952 Mechanism of turbulence. In *Proc. 2nd Midwestern Conf. of Fluid Mechanics, Ohio State University.*

THEODORSEN, T. 1954 *The Structure of Turbulence. 50 Jahre Grenzschichtforschung.* Vieweg.

TOWNSEND, A. A. 1951*a* On the fine-scale structure of turbulence. *Proc. R. Soc. Lond.* A **208**, 534–542.

TOWNSEND, A. A. 1951*b* The diffusion of heat spots in isotropic turbulence. *Proc. R. Soc. Lond.* A **209**, 418–430.

TOWNSEND, A. A. 1976 *The Structure of Turbulent Shear Flow*, 2nd edn. Cambridge University Press.

WILLMARTH, W. W. 1975 Structure of turbulence in boundary layers. *Adv. Appl. Mech.* **15**, 159–254.

WILLMARTH, W. W. 1978 Survey of multiple sensor measurements and correlations in boundary layers. In *Proc. Workshop on Coherent Structure of Turbulent Boundary Layers, Lehigh University*, p. 130.

WINANT, C. D. & BROWAND, F. K. 1974 Vortex pairing: the mechanism of turbulent mixing-layer growth at moderate Reynolds number. *J. Fluid Mech.* **63**, 237–255.